Principles and Operation of Virtual Brain Twins

Meysam Hashemi, Damien Depannemaecker, Marisa Saggio, Paul Triebkorn, Giovanni Rabuffo, Jan Fousek, Abolfazl Ziaeemehr, Viktor Sip, Anastasios Athanasiadis, Martin Breyton, et al.

Principles and Operation of Virtual Brain Twins

Meysam Hashemi[1,*,†], Damien Depannemaecker[1,†], Marisa Saggio[1,†], Paul Triebkorn[1], Giovanni Rabuffo[1], Jan Fousek[1,2], Abolfazl Ziaeemehr[1], Viktor Sip[1], Anastasios Athanasiadis[1], Martin Breyton[1,3], Marmaduke Woodman[1], Huifang Wang[1], Spase Petkoski[1], Pierpaolo Sorrentino[1,4§], Viktor Jirsa[1,*,§]

***Abstract*— Current clinical methods often overlook individual variability by relying on population-wide trials, while mechanism-based trials remain underutilized in neuroscience due to the brain's complexity. This situation may change through the use of a Virtual Brain Twin (VBT), which is a personalized digital replica of an individual's brain, integrating structural and functional brain data into advanced computational models and inference algorithms. By bridging the gap between molecular mechanisms, whole-brain dynamics, and imaging data, VBTs enhance the understanding of (patho)physiological mechanisms, advancing insights into both healthy and disordered brain function. Central to VBT is the network modeling that couples mesoscopic representation of neuronal activity through white matter connectivity, enabling the simulation of brain dynamics at a network level. This transformative approach provides interpretable predictive capabilities, supporting clinicians in personalizing treatments and optimizing interventions. This Review outlines the key components of VBT development, covering the conceptual, mathematical, technical, and clinical aspects. We describe the stages of VBT construction–from anatomical coupling and modeling to simulation and Bayesian inference–and demonstrate their applications in resting-state, healthy aging, multiple sclerosis, and epilepsy. Finally, we discuss potential extensions to other neurological disorders, such as Parkinson's disease, and explore future applications in consciousness research and brain-computer interfaces, paving the way for advancements in personalized medicine and brain-machine integration.**

"*The brain is conceived as a self-organizing system operating close to instabilities where its activities are governed by collective variables, the order parameters, that enslave the individual parts, i.e., the neurons.*" Professor Hermann Haken (1927-2024).

Abbreviations: VBT, virtual brain twin; TVB, the virtual brain; DTI, diffusion tractography imaging; DW-MRI, diffusion-weighted magnetic resonance imaging; CT, computed tomography; PET, positron emission tomography; BOLD, blood-oxygen-level-dependent; fMRI, functional magnetic resonance imaging; EEG, Electroencephalography; MEG, Magnetoencephalography; SEEG, Stereoelectroencephalography; iEEG, intracranial electroencephalography; ECoG, Electrocorticography; SC, structural connectivity; FC, functional connectivity; FCD, functional connectivity dynamic; PSD: power spectral density; NMM, Neural mass model.

I. Introduction

The Virtual Brain Twin (VBT) holds promise to aid drug discovery, tailoring of therapies, and brain-computer interface design. Currently, clinical decisions rely on population-based trials, where thousands of individuals are randomly assigned treatments. Since most trials fail, retrospective analyses attempt to distinguish responders from non-responders, often identifying causal mechanisms by chance [1]. Mechanism-based trials improved efficiency by selecting participants based on shared molecular mechanisms [2]. While effective for diseases with well-understood mechanisms (e.g., cancer), this approach is limited in neuroscience, where brain functions emerge from complex interactions across multiple scales [3], and causal models linking microscopic mechanisms to large-scale symptoms are lacking [4].

A VBT is a digital replica of an individual's brain network [5], [6], constrained by personalized structural imaging data, to simulate and make inference from functional data such as EEG, MEG, and fMRI. They encapsulate biological knowledge (e.g., neurotransmitter effects, excitatory-inhibitory interactions) in mathematical form [7]. Because they follow biological principles, these models extrapolate beyond existing data, predicting intervention outcomes or clinical status [8]–[11]. As such, therapies might be optimized based on expected outcomes. Additionally, these models can explain not only whether an intervention will work but also why.

In particular, models can be deployed to enhance the clinical management of neurological and psychiatric conditions and improve therapy delivery. Other areas of deployment might be the prediction of side effects (optimization drug therapies [12], [13]), the tailoring of non-invasive brain stimulation, and the customization of rehabilitation programs. Beyond clinical applications, mechanistic brain models deepen understanding of cognitive functions [14]. Resting-state network dynamics are crucial for diagnosing diseases by revealing how pathological states diverge from normal function. These models also tailor brain-computer interfaces, improving communication for motor-impaired individuals, and neuromorphic computing, where brain-inspired processing enhances computational efficiency.

A key example is the Virtual Epileptic Patient (VEP; [8], [9]), a whole-brain personalized model for epileptic patients, aiding treatment planning for drug-resistant cases. These models hold promise for other neurological and psychiatric disorders. Their development depends on detailed physiological knowledge. In aging, they track natural brain network changes [15]. In Alzheimer's, they aid in understanding disease progression [16]. For multiple sclerosis and Parkinson's, they offer insights into disease impact on brain connectivity [10], [11], [17]. In psychiatry, large-scale models help link neurotransmitter effects to brain dynamics [18].

This manuscript outlines the core components—conceptual, mathematical, technical, and clinical—of constructing a VBT. In section II, we introduce key ideas, covering the digital twin cycle and its components. In section III, we detail VBT building blocks, focusing on neural mass modeling, data-driven techniques, and anatomical coupling via brain connectome mapping. Then, section IV describes VBT operation, from preprocessing structural data to personalization via functional data confrontation through simulation and inference. Lastly, section V explores VBT applications, including resting state, aging, multiple sclerosis, and epilepsy, with an emphasis on their contributions to advancing clinical practice.

[1]Aix Marseille Univ, INSERM, INS, Inst Neurosci Syst, Marseille, France
[2] Central European Institute of Technology (CEITEC), Masaryk University, Brno, Czech Republic
[3] Aix Marseille Univ, APHM, INSERM, INS, Inst Neurosci Syst, Service de Pharmacologie Clinique et Pharmacosurveillance, Marseille, France
[4] Institute of Applied Sciences and Intelligent Systems, National Research Council, Pozzuoli, Italy
Corresponding authors: meysam.hashemi@univ-amu.fr, viktor.jirsa@univ-amu.fr
†These authors contributed equally. §These authors share senior authorship.

II. Concepts of Virtual Brain Twin

The Virtual Brain Twin (VBT) finds its roots in nonlinear dynamics, self-organization and synergetics [19], [20]. First efforts of building full-brain network models date back to the early 70s, when Paul Nunez discussed brain waves and global wave properties of EEG using dispersion relations, linking spatial wave lengths to temporal frequencies as observed in scalp recordings on the cm scale [21]–[23]. He linked the dispersion relation to the brain's network connectivity, specifically the exponential decay of fiber length over distance. Nunez' considerations were based on rodent data on the 1 cm scale, which he then scaled up to the human on the 10 cm scale. Nunez used this theoretical framework to quantitatively explain several features of rhythms observed in EEG. Instead of modeling multiple populations, as in the Wilson-Cowan [24] and Amari [25] field equations, the Nunez brain wave equation effectively models a single population with both excitatory and inhibitory synapses [26]. Notably, Nunez was amongst the first to integrate time delays via signal propagation into his brain wave equation, which were necessary, considering the macroscopic scale of cm [27]. The approach was fully linear, although the necessity of nonlinear pattern forming mechanisms was acknowledged. In 1996, Jirsa & Haken [28], [29] provided such a nonlinear formulation and derived a brain wave equation, which considered the split of the brain connectivity into the intracortical short-range fibers and the corticocortical long-range fiber system, which later became known as the connectome. Both fiber systems included time delays via signal propagation, albeit with different velocities. The Jirsa-Haken equation combines the linear spike-to-wave conversion at the synapses with the nonlinear wave-to-spike conversion at the cell bodies (see Walter Freeman's work on neural masses [30], [31]) and presents them in a closed form. Its initial formulation followed Nunez's approximation, in which the long-distance connectivity was modeled using an exponentially decaying integral kernel. In collaboration with Scott Kelso [32], [33], however, it became rapidly evident that many basic phenomena known from large-scale brain dynamics cannot be explained, not even as an approximation, by a spatially invariant large-scale connectivity (Figure 5**A**).

To become more concrete, let $\psi(x,t)$ be the neural vector field of dimension N capturing the population activity at time point t and position x. The dynamics of the neural field can then be described by the following integro-differential equation [28], [34]:

$$\dot{\psi}(x,t) = \mathcal{N}(\psi(x,t)) + \int_\Gamma g(\mid x - x' \mid)\mathcal{H}[\psi(x', t - \frac{\mid x - x' \mid}{c})]dx' + \int_\Gamma G(x,x')\mathcal{H}[\psi(x', t - \frac{\mid x - x' \mid}{\nu})]dx' \quad (1)$$

where $\mathcal{N}(\psi(x,t))$ is the local population model of dimension N, with N typically ranging from 1 to 12, depending on the neural mass model used. The spatial domain of the neural field is denoted by Γ, which can be one, two, or three dimensional. In the simplest one-dimensional case, $x \in \Gamma = [0, L]$ and L is the spatial length of the neural field. The homogeneous (short-range) connectivity function, $g(\mid x - x' \mid)$, is translationally invariant. If the connectivity function does not exhibit this property, it is referred to as heterogeneous, denoted as $G(x,x') \neq G(\mid x - x' \mid)$. Heterogeneous fibers are typically long-range and are myelinated, establishing the white matter of the brain. The parameters c and ν represent the propagation velocities through the homogeneous and heterogeneous connections, respectively.

To illustrate some of the properties of networks with time-delayed mixed fiber systems, assume the local neural mass dynamics to be linear, $\mathcal{N}(\psi(x,t)) = -\epsilon\psi(x,t)$, and the cortical surface to be one-dimensional with connectivity $g(\mid x - x' \mid) = \frac{1}{2\sigma}\exp(-\mid x - x' \mid)/\sigma$ (i.e., finite propagation speed, with translationally invariant connectivity). Using the method of Green's functions and applying the inverse Fourier transform, we can rewrite the above integral equations as a nonlinear partial differential equation [28], [29]:

$$\ddot{\psi} + (\omega_0^2 - c^2\Delta)\psi + 2\omega_0\dot{\psi} = (\omega_0^2 + \omega_0\frac{\partial}{\partial t})H[\psi(x,t)] \quad (2)$$

where $\omega_0 = c/\sigma > 0$ represents a characteristic frequency, and Δ denotes the Laplacian. In the absence of input, the left hand-side is a damped wave equation with oscillatory properties. The spatially uniform pattern tends to remain stable, if the slope of the sigmoid function $H[\cdot]$ on the right-hand-side is sufficiently small, though transient wave propagation may occur following small discrete perturbations [35]. If the slope exceeds a certain threshold, the spatially uniform state becomes destabilized and wave propagation may occur. Following Peter Robinson's approach [36], [37], analytic and numerical predictions for EEG spectra in terms of physiological parameters have shown agreement with empirical EEG data, considering a subcortical feedback loop that may underlie the production of the alpha rhythm [38], such as feedback through the thalamocortical projection system [39]–[41].

In absence of heterogeneous fibers, at least in an approximate manner, any activity generated at a location x_A would have to propagate through all intermediate zones to generate an activity at a distant location x_B. In the other extreme, all brain tissue is parcellated into regions with no homogeneous connectivity. Each region contracts into a point-like neural mass, compressing all information to a maximum. The outcome is a network of nodes, which are connected by the spatially variant long-range fiber system where, $G(x,x') \neq G(x - x')$. The importance of the symmetry breaking cannot be overemphasized, especially for large-scale brain networks [42]–[44]. It recognizes that, first, the topology of the network architecture is fundamental to the spatiotemporal pattern formation (Figure 5**B**), and second, the connectivity has a space-time structure, as each link of the network is characterized by a weight and a time delay relating two brain regions [45]. Breakspear et al. [46] pointed out that while global (all-to-all) coupling amongst system oscillators (e.g., Kuramoto model or generic Hopf [47]) may be a reasonable approximation for small, densely connected neural networks, it is certainly not true for large populations distributed across the cortical sheet. Instead, coupling should be spatially embedded, incorporating time delays between distant subsystems and reducing coupling strength with distance. Deco and colleagues [48], [49] have emphasized that resting-state networks emerge from a dynamic framework of noise, anatomical connectivity, and time delays. The importance of the topological component of connectivity is widely recognized nowadays [50], [51], evidenced by the many publications using graph theory and its toolboxes in neuroscience applications [3], [52]–[55]. A recent work by Pang et al. [56] further highlights this growing trend by deriving geometric eigenmodes (cortical shape) that account for the effects of local connectivity that is exponentially decaying over the geodesic distance of the cortex, i.e., the exponential distance rule [57]–[60]. The recognition of the consequences of the temporal component of connectivity is more challenging, but slowly becoming recognized. Petkoski and colleagues, for example, have demonstrated that the space-time structure of the connectivity spans a resonance body, in which brain network activity shows spectral preferences, necessitating the reformulation of traditional graph theory to account for time delays due to finite transmission speeds, and to derive a normalization of the connectome [61], [62]. When applied to the Human Connectome Project (HCP) database, this approach explains the emergence of frequency-specific networks, including

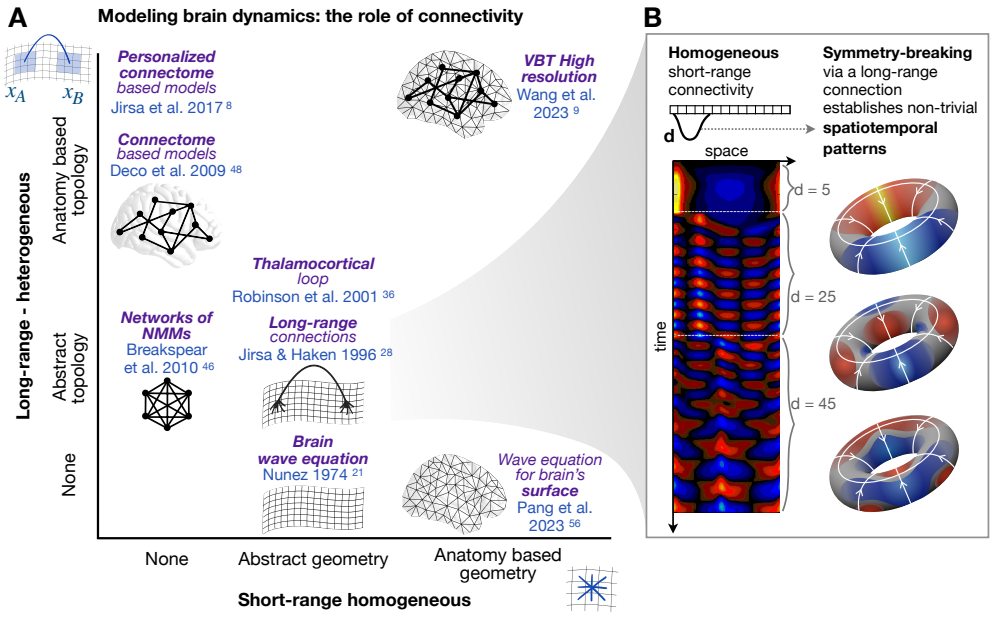

Fig. 1: **The role of homogeneous and heterogeneous connectivity in the development of models for brain activity**. (**A**) Over time the focus has shifted from homogeneous connections between neighboring nodes on the cortical surface to long-range connections among distant nodes, as described in the connectome. Technological advances have now enabled the construction of personalized brain models, incorporating both types of connectivities, as in high-resolution VBTs. We cite some exemplary references for key progresses. (**B**) Symmetry breaking of connectivity through long-range connections plays a key role in shaping non-trivial spatiotemporal dynamics. This is demonstrated in a simplified one dimensional model with a single long-range connection of length d. During the simulation, d is varied, and the system settles into new patterns. Their structure is sketched on toroidal manifolds.

the visual and default mode networks. These findings are robust across human subjects ($N = 100$) and are a fundamental network property. Although theoretically intriguing, the actual importance of the connectome's *space-time structure* in real-world applications still needs to be shown. That said, the predictive value of the individual connectome has already been demonstrated in personalized medicine. Jirsa et al. [8] have introduced personalized connectome based models to predict the outcome of surgical interventions, and assist in the clinical decision-making process through virtual surgeries [5]. Wang et al. [9] have presented a digital workflow with both low- and high-spatial resolution for mapping individual epileptogenic zone networks based on patient MRI and SEEG recordings.

At this point, it is worthwhile to pause and consider the full brain network from a theoretical perspective, returning to our initial quote by Hermann Haken [63]. Indeed, brain network activity evolves spatiotemporally within a framework, in which the nodes of the self-organizing system each experience a different pattern of interactions, that is the set of all incoming signals communicated via short- and long-range fibers, and the set of all outgoing signals. In- and outgoing interactions are not identical, as the connectivity matrix is not symmetric. Mathematically, such interaction pattern translates into spatially variant interaction kernels, which are unknown in traditional physics based on translationally invariant forces. Other networks such as airline traffic networks maybe cited to support a similar network topology comprising short- and long-range connections with the organization of network hubs, but they do not support the oscillatory wave nature of network activity as the brain does (they communicate in a particle mode, flying airplanes from one node to another). The brain's communication network thus appears to be a unique self-organizing system in this regard. Following Haken's thinking, when operating close to instabilities, in other words close to a transition from one state to another mediated by a bifurcation, low-dimensional dynamics arises in a self-organized manner. The mathematical basis is the local center manifold theorem, which explains time scale separation in the neighborhood of instabilities and provides a mechanism via adiabatic elimination to enable dimension reduction. Haken called this process enslaving, in which sets of state variables operating close to the instability show a slow dynamics, whereas the fast variables in the residual high-dimensional space are guided towards a manifold following a flow determined by the slow variables, the so-called order parameters. The time scale separation into fast and slow variables has been at the core of this mechanism underlying pattern formation. Over the past years, manifolds have found conceptual entry in the neuroscience literature, where neuronal dynamics have been visualized on manifolds using various dimensionality reduction techniques [64]–[69]. It has been argued that the role of manifolds in neurosciences goes beyond mere visualization, and that dynamics on manifolds carry computational and functional meaning. It needs to be established how the dimensionality reduction occurs in the brain, with candidate mechanisms including low-rank connectivity [70], averaging and decorrelation [42]. Jirsa & Sheheitli [42] demonstrated the emergence of structured flows on manifolds (SFM) through symmetry breaking in the low-dimensional space [71]–[73]. Dynamical systems with symmetries are called equivariant systems. Specifically for large-scale networks, it is intriguing to explore how symmetry breaking relates to the connectome. As the connectome changes during the lifespan, from neurodevelopment to neurodegeneration, and in brain disease, the formation of structured flows constrained to manifolds will be affected by these processes [15], [73]. The theoretical framework of SFMs provides a formal language in terms of dynamics to describe the effects of changes in connectivity and network nodes. In other words, the SFM is the mathematical object pertaining to the dynamics of the self-organizing process in the brain network, sufficiently general to capture multistable network states, limit cycles, travelling waves or any low-dimensional attractors. During inference, the SFM is the mathematical object sampled by the inference process. The SFM thus serves, on the one hand, to describe mechanistically spatiotemporal pattern formation processes, and, on the other hand, as a target for causal inference when investigating empirical brain imaging data. The Virtual Brain Twin (VBT) embraces both of these facets of use of SFMs, the mechanistic forward simulation and pattern generation of the large-scale brain network, and the inference using the brain network model for causal hypothesis creation. The dual use of brain modeling (simulation and inference, forward and backward) has been compulsory for the successful clinical translation and personalized medicine, establishing the workflow associated with the use of VBT.

In closure of this conceptual section, we summarize the key ingre-

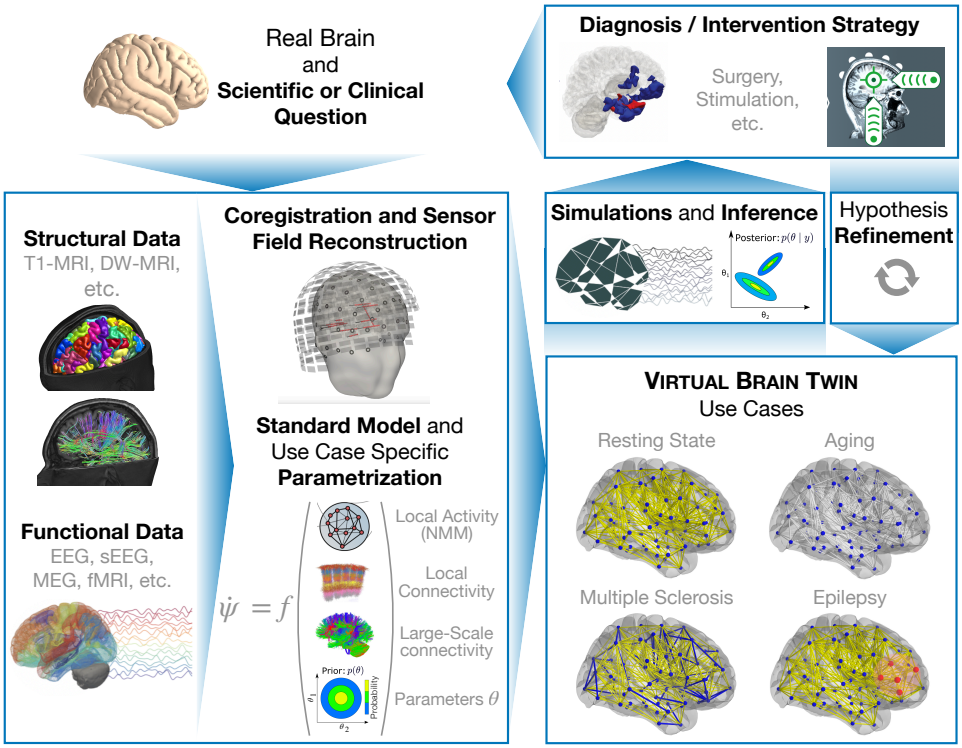

Fig. 2: **Workflow to create a Virtual Brain Twin (VBT)**: Based on scientific questions or clinical applications, appropriate structural data (such as T1-MRI, and DW-MRI) and functional data (such as EEG, SEEG, MEG, and fMRI) enable the parametrization of a standard model for a case study. The dynamical model is a nonlinear function of local activity, local connectivity, large-scale connectivity, and causal parameters. Along with source reconstruction, this allows for the creation of a VBT in which hypotheses can be tested and refined through simulations and Bayesian inference, aiding in diagnosis and interventions (such as surgery and stimulation). In this review, we demonstrate application in resting-state, healthy aging, multiple sclerosis, and epilepsy.

dients of the VBT: it is the digital representation of an individual's brain as a full-brain network model, which integrates the same individual's structural and functional brain imaging data in the model building (hence "Twin"). The process of creating a VBT comprises three stages (see Figure 2): first, structural brain imaging data (MRI, DTI, eventually CT) are co-registered in the same space. MRI data are parcellated into nodes, which, depending on the desired resolution, may vary from 10 cm^2 and hundreds of nodes, to 1 mm^2 and hundred thousands of vertices. In the former case, a brain region typically equals a node, whereas in the latter case a brain region spans hundreds of vertices. Tractography is performed from the DTI data to create the individual's connectome. The nodes are connected through the connectome to a network, which is spanned in physical space. This step is critical, as it allows to position correctly the brain imaging sensors in the same space. Depending on the brain imaging modality, sensors are EEG contacts, MEG SQUIDs, and voxels in fMRI. The source-to-sensor mapping is computed from the relevant physics equations. Second, each node is equipped with a neural mass model (NMM), which is a reduced mathematical representation of the dynamical equations prescribing the behavior of large populations of neurons, typically at least several hundred thousands. Neural masses still maintain the multiscale nature of the processes ongoing in a neuronal population such as fast neuronal discharges and the slower chemical processes such as extracellular potassium changes. The connectome provides the connectivity matrix linking the activity across nodes through white-matter tracts. At high spatial resolution, the vertices in a brain region integrate the connectivity within the cortical areas in addition to the highly heterogeneous connectivity between the brain regions, the so-called connectome. Third, using functional brain imaging data, the application of Bayesian inference methods provides an estimation of relevant model parameters. Typically, not all parameters are inferred. Most of them are set into operating ranges from the literature based on physiological estimates or mathematical calculations. The only inferred parameters are those that are relevant to the intended use of the VBT, typically linked to some pathophysiological cause in clinical applications, for instance the epileptogenic zone in epilepsy or lesions in multiple sclerosis. This approach supports the convergence of the inference process.

III. Building the Virtual Brain Twin: Nodes and Connectome

In the following sections, we will describe the process of building the VBT, reviewing NMMs for a node's dynamics, connecting them to formulate connectome-based models at low- and high-resolutions, and outlining the methodology for mapping from source level to sensor measurements.

A. Neural Mass Models as network nodes

Neural mass models (NMMs) represent the activity of large populations of strongly interconnected neurons, corresponding to the mesoscopic scale, which lies between the microscopic cellular level and macroscopic whole-brain models [90]. These models capture the population dynamics by describing the evolution of a few collective mesoscopic variables, such as mean potential or firing rate, through the use of differential equations. This is conceptually analogous to describing the velocities of gas molecules using temperature as a collective variable, even though in the case of neural activity, the intermediate steps linking the two levels of description are far less understood.

Empirical recordings of brain activity at the whole brain level are only possible with very limited spatial (or temporal) resolution. High spatial resolution, up to $\sim mm^3$ resolution [91], [92], can be achieved using fMRI. Even in this best-case scenario, it is estimated that a single fMRI voxel contains $\sim 500k$ interconnected neurons [93], which form complex interactions on their own, making it intractable to infer the causal links between neuronal organization and whole-brain activity. This focus on the mesoscopic scale thus aligns well with the practical considerations and needs of clinical applications: in translational contexts, the mesoscopic scale is the most

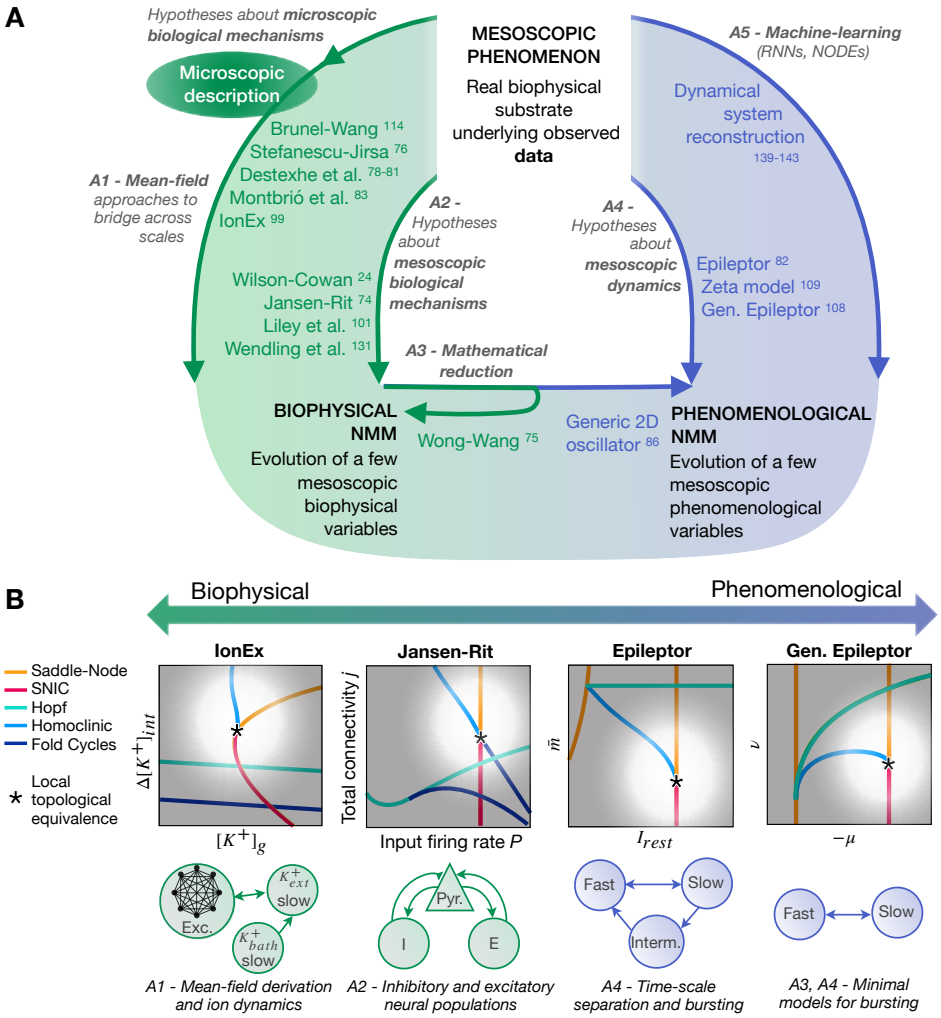

Fig. 3: **Neural Mass Models (NMMs).** (**A**) Main approaches to build NMMs, with specific models applying them at varying degrees and lying on the continuum between biological and phenomenologically inspired. For biophysical models, hypotheses can be cast also at the microscopic level and be followed by the application of mean-field methods to derive the mesoscopic model (A1), or the hypotheses can be advanced directly at the mesoscopic scale (A2). Biophysical NMMs can also be obtained through the mathematical reduction of more complex models (A3). The latter approach can be used to obtain a phenomenological model reproducing key dynamical features of a biophysical one (A3). Another route to phenomenological models is to start directly from data and implement hypotheses about the mesoscopic dynamics (A4) or by applying machine-learning approaches (A5). This leads to models with different characteristics (see Table I) tailored to specific applications. (**B**) Despite this heterogeneity, models can share some core dynamical mechanisms, allowing for a bridge between them. Here we show examples from seizure modeling. A specific structure in their bifurcation diagram (top row, white region surrounding the asterisk), enables seizures in all these models. However, the approaches to modeling are quite diverse, as is the interpretation of variables and parameters.

TABLE I: **Examples of commonly used Neural Mass Models (NMMs), in the context of VBT**. These models are associated with the corresponding approaches presented in Figure 3: A1: Mean-field methods from microscopic hypotheses, A2: Mesoscopic-scale hypotheses, A3: Mathematical reduction from biophysical or phenomenological models, A4: Data-driven mesoscopic hypotheses, A5: Machine-learning models. Models' variables encode various aspects of brain dynamics, which can involve different separate timescales. With more than two timescales, behaviors such as mixed-mode oscillations or bursting become possible.

Model	Derivation	# Timescales	Repertoire	Number and Interpretation of Variables
Wilson-Cowan, 1972 [24]	A2 - first mesoscopic description of interacting excitatory and inhibitory populations	1	up/down, oscillations	#2; firing rates of two populations (Excitatory and Inhibitory)
Jansen-Rit, 1995 [74]	A2 - extends Wilson-Cowan model to three populations	1	up/down, coexisting oscillations (related to high alpha and low beta EEG oscillations)	#6; membrane potentials and firing rates of pyramidal neurons, excitatory, and inhibitory interneurons
Wong-Wang, 2006 [75]	A3 - reduction from biophysical model of interaction of excitatory and inhibitory populations	1	multi-stability	#2; synaptic gating variable of the excitatory and inhibitory populations
Stefanescu-Jirsa 2/3D, 2008 [76]	A1 - dispersion of parameters causes clustering of neurons (FitzHugh–Nagumo / Hindmarsh–Rose) [77]	1 or 2	up/down, oscillations /bursting	#2; or #3; state variables representing excitatory and inhibitory interactions
Destexhe et al., 2009-2024 [78]–[81]	A1 - based on transfer function obtained from several neuron models or recordings	1 or 2 (with adaptation)	up/down, additional stable fixed point	#3 (#6; with 2nd order); fast-spiking inhibitory and regular-spiking excitatory firing rates + adaptation (+ 2nd order)
Epileptor [82]	A4 - slow variable mechanisms to start and stop seizures through specific bifurcations to produce precital spikes and spike-and-wave complexes through an excitable system	3	up/down, oscillations, bursting	#6 field potential as a combination of phenomenological variables acting on different timescales
Montbrió et al., 2015 [83]	A1 - starts from a network of QIF neurons, exact assuming the Lorentzian ansatz	1	up/down	#2; mean-membrane and firing rate of an excitatory population
Depannemaecker et al., 2024 [84]	A1 - extends the aQIF-MF model (Chen & Campbell [85]) to include dopamine dynamics	3	up/down, bursting	#8; firing rate, mean membrane potential, adaptation, inhibitory and excitatory synaptic activations, dopamine receptor activation, local dopamine concentration
Generic 2D [86]	A3-A4 - extends the dynamics of single neurons (FitzHugh-Nagumo Model [87], [88], Morris-Lecar [89])	2	up/down, oscillations	#2; membrane potential, and a recovery or damping variable

accessible and measurable, through techniques such as EEG, MEG or fMRI, making it the natural target for data collection and analysis. By prioritizing this scale and the related emergent properties of brain dynamics, models can be directly applied to clinical settings, offering actionable insights while bypassing the complexity of microscopic-level details and their potentially degenerate mapping to mesoscopic activity [94]. This latter point pertains to the ability to generalize across systems where different microscopic configurations can lead to the same emergent global dynamics. This is called degeneracy, which is the geometrical counterpart of non-identifiability [95]. In other words, while the microscopic realizations may differ, they do not necessarily affect the system's overarching behavior, enabling the development of models without the need to precisely capture every fine detail. In addition, this formidable information compression makes it computationally feasible to simulate whole-brain activity in a personalized fashion for clinical applications [7], [96].

There are several routes to designing NMMs, each providing unique insights into the modeling of brain activity (Figure 3**A**). When specific biological assumptions and constraints are incorporated, ensuring that the model's variables maintain an explicit link to the underlying physiology, we refer to these as biophysically inspired or mechanistic models [97]. When the focus is rather on directly reproducing the phenomenon of interest and making hypotheses about the underlying dynamics, we deal with phenomenological models of abstract variables and parameters. These dynamics can also be inferred through data-driven machine learning approaches (see subsubsection III-A.5). Indeed, there exists a continuum of different models, ranging from the most mechanistic and detailed model to the most reduced and phenomenological one. The different components of the model can encode different levels of biophysical or phenomenological description, providing more detail on the mechanisms of interest for a given study or application. This variety in modeling approaches allows to choose the appropriate level of abstraction based on specific needs [98]. In addition, phenomenological models can identify dynamical structures, that is key features of the differential equations allowing the system to exhibit certain behaviors, that can be related and mapped onto the dynamics of more detailed biophysical models [98], [99]. In this way, they build the bridge between biological mechanisms and emergent dynamics (Figure 3**B**).

The question of which are the possible behaviors of a system is tightly linked to which are the stable solutions of the related differential equations. We refer to [96], [100] for a short introduction to this topic, and here only recall some key concepts useful in the following review of NMMs. When, after a transient, the activity of a system stabilizes to some specific pattern, we say that the system has reached an *attractor.* If the system is slightly perturbed from the attractor, it will move back towards it (hence the name). Attractors can be as simple as all variables stabilizing at constant values: these are called *fixed points*. An example is the resting membrane potential of a neuron. The system can also stabilize into a periodic behavior, in this case the attractor is called *limit cycle*. An example is given by sustained neuronal oscillations. Limit cycles can have complex shapes giving rise to more involved timeseries, as for example in spike and wave complexes. Usually, the repertoire of possible behaviors of a system depends on the values of some parameters (e.g. linked to neuromodulation). If, when varying a certain parameter, this repertoire changes qualitatively, we say that the system has undergone a *bifurcation*.

1) Biophysically inspired models: The mechanisms of biophysically inspired models can be directly motivated at the mesoscopic scale. In the simplified example of the gas, this would correspond to directly describe how temperature would evolve under certain conditions. Examples are the seminal Wilson-Cowan model of two interacting excitatory and inhibitory neural populations [24], and its extensions [74], [101], inspiring transfer function-based mean-field approaches [78], [80], [81]. The model's equations can alternatively be derived by applying mean-field theory to networks of coupled neurons [26] in the spirit of statistical physics, to explicitly derive the link between micro and mesoscopic variables. In the gas example, this would involve starting from the equations that describe the velocity of each molecule and formally working up to the average behavior, i.e. temperature. For neural activity under a series of assumptions, this approach yields the behavior of the mean of the population activity and, potentially, of the higher momenta [90]. A special class of these models, referred to as next-generation NMMs [102], [103], relies on the assumption of all-to-all connected neurons with heterogeneity following a Lorentzian distribution. This approach provides an exact derivation for infinitely large networks (in the thermodynamics limit, i.e., $N \to \infty$) [83], [85], [104], and accounts for the degree of within population synchrony. The original approach developed by Montbrió et al. [83] for population of quadratic integrate-and-fire (QIF) neurons, and has been extended to account for physiological factors such as adaptation [85], or ionic exchange [99]. To exemplify some key features of NMMs, we briefly describe the first of these next-generation NMMs, given by [83], which is a minimal representation upon which the other derivations add extra complexity and biological realism. The model reads:

$$\begin{aligned} \dot{r} &= 2rv + \frac{\Delta}{\pi} \\ \dot{v} &= v^2 - \pi^2 r^2 + Jr + \eta + I(t) \end{aligned} \tag{3}$$

where r, and v represent the mean firing rate and the mean neuronal membrane potential of the population, respectively. The parameter J denotes the synaptic weight, η is the average excitability, and Δ indicates the spread of the neuronal excitability distribution in the neural population.

The NNM of Montbrió et al. (given by Equation 3) imposes a flow in the low-dimensional space spanned by the system's variables (i.e., how the system's dynamics evolve in state space) (Figure 4, top). For certain parameter settings, the model demonstrates bistability between two fixed points, characterized by the coexistence of a lower firing rate regime (down-state) and a higher firing rate regime (up-state). This feature, the coexistence of two attractors in state space, is common to several NMMs [24], [74]–[76], [78], [82], [101], [105]–[110], and is crucial for capturing key characteristics in empirical data, such as functional connectivity dynamics and neuronal cascades [111], [112]. The up-state often facilitates oscillatory activity, which can be either damped, as seen in the next-generation NMMs [83], where it is a spiral fixed point (Figure 4, top), or sustained when it is surrounded by a a limit cycle (Figure 4, bottom) [24], [76], [82], [113]. Some models even allow for the coexistence of limit cycles in addition to the down-state, accounting for the presence of different frequency bands in the EEG [74], [101]. The attractors' repertoire for some common models is summarized in Table I. Transitions between coexisting attractors can occur due to noise or inputs strong enough to force the system across a *separatrix* and into the basin of attraction of a different attractor. Alternatively transitions can occur through the disappearance of the current attractor, forcing the system to reach another available one. The two mechanisms, noise/input induced transitions and bifurcations, are shown in Figure 4 (top and bottom, respectively).

2) Phenomenological models: The complete set of attractors and bifurcations, that is the bifurcation diagram, provides a powerful description of the dynamical repertoire of a model. Models derived from different approaches can share core properties of the bifurcation diagrams, such as the bistability between down-state and up-state

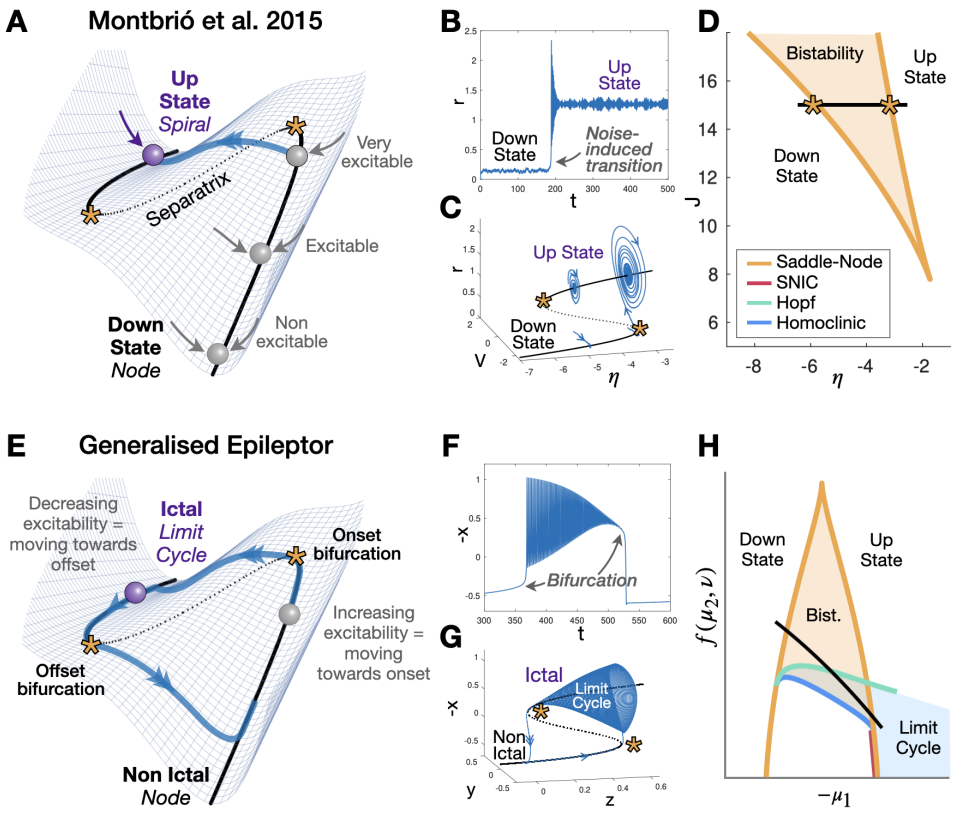

Fig. 4: **Bistability and slow dynamics in NMMs.** (**A**) Attractors (black lines) can be thought as the bottom of valleys in a landcape: a ball rolls downhill and settles there as a system behavior settles into an attractor. The top of the hill (dashed black) separates the initial conditions making the ball roll towards each attractor. In the Montbrio et al model, these attractors are fixed points. If the system is in the down state, an input can push it across the sepratrix so that the system moves (spiriling in this case) to the upstate. Smaller inputs causes the transition the closer the down state is to the separatrix. (**B**) Timeseries for this transition. (**C**) Bifurcation diagram showing how attractors change with the excitability parameter η. (**D**) The bifurcation values (orange curves) also depend on the other parameter J. A black segment marks the value $J = 15$ used in panels (*B-C*), and we set $\Delta = 1$. (**E**) Bistability between a fixed point and a limit cycle allows to model seizures. Transitions can again be triggered by inputs. The Epileptor model instead, endows the excitability parameter, z, with slow dynamics so that it pushes the initially non ictal system towards the onset bifurcation causing this state to disappear. The system is forced to move towards the other attractor: the ictal oscillatory state. This causes a reversal in the movement of z until the offset bifurcation is met and the system settles back to rest. Timeseries (**F**) and bifurcation diagrams (**G-H**). We plot $-x$ to keep the analogy with the Montbrio model, but the ictal state has a lower baseline than the interictal one, consistently with Direct Current EEG recordings.

described earlier, identifying these as key features of NMMs. When dynamical systems share these properties, they display the same variation of phase flow in the state space, which allows to find a homeomorphism transforming one dynamical system into another. This justifies the use of mathematical methods to derive reduced phenomenological models that account for these crucial dynamical features in a more analytically and computationally tractable manner (Figure 3**A**). An example is the Wong-Wang model [75], which is derived under the adiabatic approximation [42] from the Brunel-Wang model [114] for a cortical network dominated by recurrent inhibition. Another approach to developing phenomenological models involves formulating hypotheses about the dynamical mechanisms–rather than the biophysical ones–that underlie specific features observed in the data [100]. This approach has proven successful, for example, in the modeling of epileptic seizures [82] or interictal spikes [115].

Given that the Virtual Epileptic Patient (VEP; [5], [8], [9]) is currently the most advanced application of the VBTs, we will devote the next section to an overview of NMMs for seizures, with a particular focus on the model of choice for the VEP, the phenomenological Epileptor [82].

3) Seizure NMMs for VBT: The dimensionality reduction in the mesoscopic description is particularly justified in models of epileptic seizures, which are events characterized by a high degree of neuronal coordination. Among the models for seizures [98], [100], [116], those used for the region dynamics within large-scale personalized simulations mainly focus on the onset of seizures and on their propagation throughout the brain due to coupling among regions [115], [117]–[122]. The key features of most of these models are: the presence of two attractors–one for the interictal and the other the ictal state; a mechanism for transitions between these attractors; an excitability parameter characterizing how prone the system is to undergo a transitions; and a specific pair of bifurcations that destabilize the interictal/ictal states, influencing the overall dynamics of the model (as shown in Figure 4, bottom).

In more details, a fixed-point is used to represent the interictal (healthy), regime while a limit cycle is used for the ictal regime; in some cases, this is further reduced to another fixed point [121], [123]. Common dynamical mechanisms for seizure onset include [100], [124]–[126]: input- or noise-induced transitions among coexisting attractors (i.e., in the presence of bistability); and bifurcations that lead to the destabilization of the interictal state, when the bifurcation parameter is allowed to change due to noise or slow dynamics. Bistability is not required for bifurcations to occur, however, its presence can be exploited to produce hysteresis-loop bursting [127]. This provides a mechanism to autonomously produce seizures that does not rely on noise, thanks to feedback between fast and slow variables. This concept is central to the Epileptor model [82]. Another key characteristic of seizure models is the presence of a single parameter, generically referred to as excitability, that can be used to differentiate healthy and unhealthy brain regions and serves as the target for personalization at the NMM level, hence as a generative parameter in the inference process.

Finally, different bifurcations leading to the destabilization of the interictal/ictal state exhibit specific signatures in the time series, for instance, the presence/absence of a baseline shift, or characteristic trends in the amplitude and frequency behaviors. These can significantly affect the dynamical properties of the model, including synchronizability or responsiveness to stimulation [82], [127], [128].

4) Epileptor: Despite the multi-factorial causes of epilepsy and the heterogeneity of its clinical manifestation, electrographic seizures display remarkably stereotyped features, consistent across species and even in small neuronal preparations [82]. Jirsa and colleagues

studied these features, identified the signatures of specific bifurcations at seizure onset and offset, and proposed a taxonomy of seizures based on such bifurcations pairs, which they called dynamotypes [82], [108], [127], [128]. They phenomenologically modeled the most common class in the Epileptor, incorporating systems that operate on three timescales: a fast subsystem, which displays the healthy fixed point and the limit cycle for fast ictal oscillations; a slow variable responsible for the transitions across attractors in the fast subsystem; and an intermediate subsystem, encoding both preictal spikes and spike-and-wave complexes. While the Epileptor is typically used in the slow variable regime, its parameters can be adjusted to accommodate both bistability and monostability [129], as well as transitions induced by input, noise, or slow variable–including mixed scenarios for seizure onset/offset [82], [130]– without altering the excitability parameter. Interestingly, the bifurcation diagram of the Epileptor shares core features with several biophysical models developed for epilepsy [99], [131], [132] (Figure 3**B**). Beyond modeling seizure onset and offset mechanisms, the Epileptor can also replicate phenomena such as status epilepticus and depolarization block [133]. The model can be further extended by including two neuronal subpopulations of epileptogenic and nonepileptogenic type, to make it capable of producing physiological oscillations in addition to the epileptiform activity [115].

The Epileptor has been designed to target one dynamotype, while patients also experience seizures that align with other classes [82], [128]. Some of these can be accounted for by adjusting the parameters of the Epileptor [130], while these and others can be more generically modeled using unfolding theory [108], [134], [135]. This approach yields a simplified model with two fast variables and a slow one:

$$\begin{aligned} \dot{x} &= -y \\ \dot{y} &= x^3 - \mu_2(z)x - \mu_1(z) - y(\nu(z) + x + x^2) \\ \dot{z} &= -c(\sqrt{(x - x_s(z))^2 + y^2} - d^*) \end{aligned} \tag{4}$$

with $c \ll 1$. The slow variable z pushes the fast subsystem (x, y) along a trajectory $(\mu_1(z)), \mu_2(z), \nu(z))$ in parameter space, potentially crossing different bifurcations sequences, and generating seizures corresponding to specific classes. We refer to this model as Generalized Epileptor (Figure 4, bottom) and the subset of bifurcation curves it shares with the Epileptor are shown in (Figure 4H).

5) Data-driven models: Given the complexity of biological neural systems, designing a low-dimensional model aiming to capture the important features of neural dynamics is a difficult task, whether following a more phenomenological or biophysical approach. Such task necessarily involves introducing some strong assumptions and approximations, whose applicability can be questioned. Modern machine learning, however, opens an alternative way; one that relies on experimental data and training techniques to learn the underlying dynamics. Such data-driven approaches can be understood as an extreme variant of phenomenological models, where the phenomena to be modeled are extracted from the experimental data automatically by appropriately designed training algorithms.

Data-driven models can also be used for model order reduction [136]. With this approach, a low-dimensional model is trained on data generated by a high-dimensional, computationally costly model– such as a model of large biologically realistic neuronal networks with single neuron resolution. The successfully trained low-dimensional model then captures the phase flows in state space generated by the high-dimensional model and thus serves as a first approximation of the latter's emergent dynamics.

A range of methods for extracting the dynamics from data has been proposed and used. Approaches based on linear state space models are theoretically well understood and can be efficiently trained [137], but are inherently limited in the nature of the dynamics they can represent. Even so, they provide a good baseline to evaluate more complex models of brain dynamics [138]. Recurrent neural networks (RNNs) are much more flexible, and are widely used for dynamical system reconstruction in neuroscience [139]. Their main building block is a state vector, supplemented by an update mechanism usually in form of some combination of matrix multiplications and element-wise nonlinearities. Popular variants include architectures designed for better performance on problems with long term dependencies such as Long Short-Term Memory (LSTM; [140]) or Gated Recurrent Unit (GRU) networks [141].

An approach related to RNNs is Neural Ordinary Differential Equations (NODEs; [142]), where the gradients of the loss function are calculated via adjoint method in continuous time, avoiding the use of memory-intensive backpropagation, and allowing the use of solvers with adaptive time steps. The disadvantages of RNNs include potentially difficult interpretation, since the trained system is not in the form of simple equations easily understood by humans. Better interpretability is the goal of the SINDy method [143], which approximates the system by a linear combination of pre-specified basis functions such as polynomials, and optimizes for sparsity in this representation. However, this approach faces challenges such as noise sensitivity, reliance on an appropriate function library, and balancing model sparsity with accuracy. Additionally, it struggles with highly nonlinear systems and encounters scalability issues in high-dimensional settings due to computational costs. Finally, sometimes a specific dynamical nature of a problem can be exploited to build a problem-specific form of a data-driven model, such as the network model of spreading epileptic seizures [144].

In the context of network-based brain modeling, the low-dimensional neural mass models can be trained either in isolation or embedded in the network. The former can be justified if the experimental data can be obtained from isolated tissue, or when trained on simulated data from a larger model where the interregional coupling is either known or absent [145]. The trained neural mass models are then coupled together to form the whole-brain model using the methodology outlined in the next sections. In the latter case, the low-dimensional models are first coupled with the known structural network, and then their dynamics is trained jointly [146].

B. Connectome-based brain networks

Connectome-based models are a well-established approach for investigating functional neuroimaging modalities such as fMRI, MEG, and EEG [3], [45], [55], [86]. This network-based modeling incorporates individual structural brain imaging data [147], typically diffusion-weighted imaging data, to estimate the edge weights and lengths [148]. The structural connectivity imposes a constraint on the brain dynamics, allowing for the personalized simulation of the brain's (ab)normal activities and their associated imaging recordings, potentially informing targeted interventions [5], [7], [9]. In the following subsections, we describe this approach in both low resolution (neural mass modeling) and high resolution (neural field approach).

1) Networks with neural nodes at low resolution: At the coarser level of brain regions, the brain network dynamics are described as

$$\dot{\psi}_{\mathbf{i}}(t) = \mathcal{N}(\psi_{\mathbf{i}}) + G\sum_{j=1}^{N} \mathrm{w}_{ij}\mathcal{H}(\psi_i, \psi_j(t - \tau_{ij})) + z(\psi_{\mathbf{i}})\xi_i(t), \tag{5}$$

where $i = 1, 2, \ldots, N$, with N being the number of brain regions. The evolution of local neural activity $\psi_i(t)$ in region i when uncoupled is driven by the inherent neuronal activity represented through the nonlinear function of the neuronal mass model $\mathcal{N}(\psi_{\mathbf{i}})$. Additionally, when constructing the brain network model, the connectome-

based architecture dictates the strength and delay of the interactions between brain areas through the coupling function $\mathcal{H}(\psi_i, \psi_j(t-\tau_{ij}))$. Here, the axonal transmission introduces delays in the neuronal activity of distant regions, $\tau_{i,j}$, and the strength of this coupling is determined by the connectome weights w_{ij}. These are typically estimated by tractography based on diffusion weighted MRI [149]. Such a coarser representation of the brain network includes only the heterogeneous connectivity from the connectome, while local connections are assumed to be part of the neural mass models. Finally, there is a noise term in the dynamics that can depend on neuronal activity through the function z, which multiplies a Gaussian with independent time series characterized by $\langle \xi_i(t) \rangle = 0$ and $\langle \xi_i(t)\xi_j(t') \rangle = 2D\delta(t-t')\delta_{i,j}$. Note that, in general, the working point of the system is determined by the interplay between the global coupling G, local (bifurcation) parameters, and the noise strength D. Time delays and weights constitute the space-time structure of connectivity, which is crucial in shaping its macroscopic activity [45], [61], [86], [150], including the phase relationships between brain regions [151]. Their impact can be unified in the so-called normalization of the connectome [62] that allows graph-theoretical metrics to unveil structural affinities for spectrally-dependent activation patterns in the brain.

2) Networks with neural fields at high resolution: To achieve a more spatially resolved activity of the brain, the driving Equation 5 requires to be modified to also include the interactions from the nearby tissue:

$$\dot{\psi}(x,t) = \mathcal{N}(\psi(x,t)) + \int_{\Gamma_{local}} g(\mid x - x' \mid)\mathcal{H}[\psi(x')]dx' + \quad (6)$$
$$\int_{\Gamma_{global}} G(x,x')\mathcal{H}[\psi(x', t - \frac{\mid x - x' \mid}{\nu})]dx' + z(\psi(x,t))\xi(t),$$

where, the neural activity $\psi(x,t)$ at position x and time t is now also influenced by the short-range intracortical synaptic connections, which are instantaneous (i.e., $c \to \infty$ in Equation 1). This assumes that neural populations across the cortical surface are connected to their neighbouring populations in a distance-dependent manner, as described by neural field theory [7], [28], [152]. To account for this in the model, the spatial resolution is increased. While in the brain network representation Equation 5, atlas-derived brain regions on the cortex could be collapsed to a single point (or node) in the network, the model now describes positions x as points on the unfolded cortical surface Γ_{local}, as extracted from structural MRI. Typically local connection strength is assumed to decay with increasing distance and to be translationally invariant. Thus, a kernel is chosen and applied on the geodesic distances between points x and x' on the cortex to obtain $g(\mid x - x' \mid)$. Common choices are Gaussian or exponential decay kernels, parameterized to limit the effective connection strengths to a few centimeters or millimeters.

In addition to the short-range, the long-range connectivity can now be represented as an integral over the spatial domain Γ_{global}, extending across the whole brain. Assuming the heterogeneous two-point connection, $G(x,x') = \sum_{i,j=1}^{2} w_{ij}\delta(x-x_i)\delta(x'-x_j), \quad i \neq j$, where $w_{ij} \in \mathbb{R}$ represents the coupling strength through the heterogeneous connection [28], [152]. In the discretized version of the model, this increase in spatial resolution raises the number of positions x, from around 200 regions defined by the atlas to the number of vertices of the cortical surface mesh, which can commonly range up to 200 thousands. Thus, given a typical adult brain, a node of the connectome would approximate the neural activity of around 10 cm^2 of the cortical surface, while with neural fields a single vertex represents around 1 mm^2.

This increase in resolution results in a substantial increase in computational cost, potentially limiting the usability of the model, due to the formidable challenges it introduces for model inversion. Approximately 25000 iterations per second for the neural field simulation and 25 million iterations per second for the neural mass, representing a 3 orders of magnitude difference, were achieved on a state-of-the-art desktop GPU, the RTX 4090. Nevertheless, the pseudo-spectral approach [153] and reparameterizing the parameter space into spherical harmonic mode coefficients [154] can be employed to reduce the computational burden and facilitate the inference process. With this increase in resolution, certain empirically observed phenomena like cortical traveling waves [155] can be described. High spatial resolution is also essential for accurately modeling electric fields generated by neural sources or brain stimulation electrodes [5], [156].

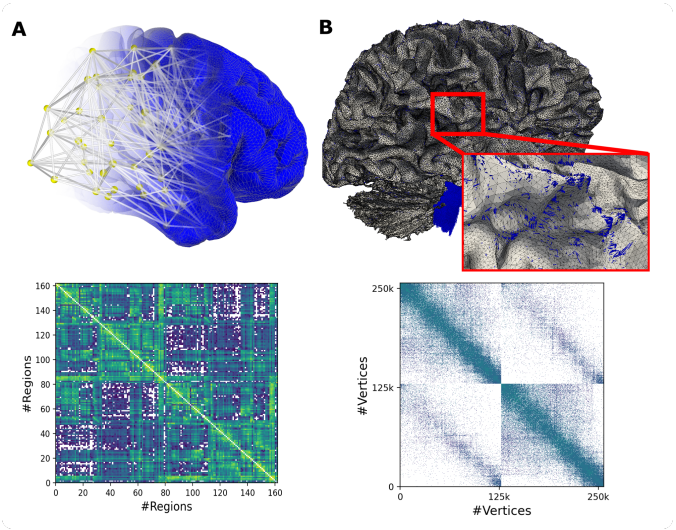

Fig. 5: **The low- and high-resolution simulations in VBTs**. (**A**) The network with a neural mass model at low resolution, showing the 3D brain network (top) and connectivity between 162 regions (bottom). (**B**) The network as a neural field model at high resolution, showing cortical surface with streamline intersections (top) and derived connectivity between 260k vertices (bottom).

C. Mapping neural sources to sensors

The neural activity $\psi(x,t)$, simulated via Equation 5 and Equation 6, is not directly observable in real world experiments. Therefore, a projection needs to be established to transform the simulated neural activity into empirically measurable quantities, such as BOLD fMRI, EEG, MEG or iEEG.

In fMRI, the BOLD signal reflects deoxyhemoglobin levels in tissue. Due to its paramagnetic properties, deoxyhemoglobin creates magnetic field gradients around blood vessels, reducing the MR signal. Changes in deoxyhemoglobin concentration are linked to neural activity through neurovascular coupling [157]. Various cellular and molecular mechanisms, including the release of neurotransmitters, ions, and metabolic byproducts, trigger vasodilation and increase blood flow [158]. The BOLD signal response to a brief stimulus follows the hemodynamic response function. It begins at baseline, peaks around 5 seconds after stimulus onset, dips below baseline into an undershoot at approximately 10 seconds, and returns to baseline within 20-30 seconds [159]. The Balloon-Windkessel model describes the hemodynamic response to neural activity $\psi(x_i,t)$, which drives the BOLD signal [159]. It consists of a set of nonlinear differential equations that link neural activity to regional cerebral blood flow, blood volume, and deoxyhemoglobin levels. Through neurovascular

coupling, neural activation increases blood inflow to a region, expanding blood vessels like a "balloon". Meanwhile, blood outflow is regulated by the vessels acting as a "Windkessel", with higher outflows occurring when the vessels are more distended. The overall blood volume is determined by the balance of inflow and outflow, while deoxyhemoglobin levels depend on both oxygen extraction from inflowing blood and the amount of blood leaving the region. Ultimately, the BOLD signal itself is a nonlinear function of blood volume, oxygen metabolism, and deoxyhemoglobin concentration [159], [160]. While the earlier Balloon-Windkessel model assumed vasodilation of the venous system, more recent evidence suggests that dilation mainly occurs in the arterioles, leading to new hemodynamic models [161]. Similarly, improvements in the temporal and spatial resolution of fMRI imaging technology will require adaptations to hemodynamic models [162]. Furthermore, empirical evidence suggests that the hemodynamic response varies across brain regions and individuals, which may impact the prediction of functional connectivity [163], [164]. Additionally, neurovascular coupling is often impaired in neurodegenerative disease, which may contribute to observed functional connectivity [165]. Similarly, the hemodynamic response changes with healthy aging [166]. Most studies using brain network modeling to predict functional connectivity so far have used a single hemodynamic model across all brain regions, subjects, and conditions. This is probably a shortcoming of current studies. Future studies should investigate varying hemodynamic models to potentially enhance the accuracy of functional connectivity predictions.

For EEG, MEG and SEEG, a projection can be calculated by solving the electromagnetic forward problem. The forward model combines location and orientation of electromagnetic sources and sensors with a volume conductor model. The main source for the measurable electromagnetic field is the synchronous synaptic activity of groups of parallel-aligned cortical pyramidal neurons [167]. These synaptic transmembrane ion currents are approximated by a current dipole, positioned on and oriented orthogonally to the cortical surface, which can be extracted from a subject's structural MRI. The volume conductor is a three-dimensional model that describes the conductive properties of the extracellular tissue, including compartments such as the brain, cerebrospinal fluid, skull and skin. Next, the sensor locations are aligned with the volume conductor and source model. Finally, the electric potential and magnetic induction at the sensors is calculated by solving Maxwell's equation in its quasistatic approximation. In its simplest form, the volume conductor can be assumed to represent an unbounded and homogeneous medium, for which analytic solutions to Maxwell's equation exist [168]. This assumption may be reasonable for intracortical sensors like SEEG, which are from any tissue boundaries and thus boundary effects may be neglected. For EEG and MEG, however, changes of conductivity impact the measured signal. In the simplest case, one- or three-layered spherical models, fitted to the head shape and sensors, have been applied. More advanced numerical approaches, such as boundary element methods (BEM) and finite element methods (FEM), use subject-specific geometries extracted from structural MRI for more accurate modeling [169], [170]. The BEM often considers three boundary surfaces: scalp-air, skull-scalp, and skull-brain. Conductivity within each compartment is assumed to be homogenous and isotropic. In FEMs, the whole head volume is tesselated into tetrahedra, and a unique conductivity tensor can be specified for each tetrahedra separately. This allows to account for anistropic conductances in skull and white matter [171]. Further improvements can be achieved through biophysically realistic forward modeling, allowing for multiple dipoles, especially for sensors close to the neural sources, i.e., ECoG [172]. There are multiple openly available software suites which can be used to compute the forward model and to perform general analysis of empirical data, such as MNE [173], Brainstorm [174], FieldTrip [175], OpenMEEG [176].

IV. Operating the Virtual Brain Twin: Technologies

In the following sections, we will detail the steps and technologies involved in operating the VBTs, starting with the preprocessing of structural data, construction of brain atlases, and coregistration to build individualized brain network models. This will be followed by an explanation of the simulation process and the inference techniques used to confront the VBTs with functional data.

A. Preprocessing, atlases and coregistration

Reconstructing virtual brains from neuroimaging data entails processing of multiple imaging modalities, including structural MRI (T1w and T2w images), diffusion weighted MRI, functional MRI, potentially CT scans, PET, and EEG/MEG/SEEG and additional modalities as applicable. The aim of the processing is to obtain the structural scaffold of a subject's virtual brain, and processed functional data as a target for inference, against which dynamics of the model can be compared. The scientific field of image preprocessing is extensive, and we here point towards reviews from this field to give a broad overview. Preprocessing of diffusion weighted images involves a multitude of steps for denoising and artefact correction [177], followed by streamline tractography to estimate the white matter connections [149]. Subsequently streamlines are grouped according to some brain atlas [178] to obtain the structural connectome [179]. Furthermore, depending on the use case, post-SEEG implantation CT [180] or EEG-electrode MRI images [181] are aligned with the different imaging modalities to allow for an accurate electromagnetic forward model. Similarly, functional data like fMRI [182], [183] and EEG/MEG [184] are artefact corrected and aligned with the structural data. Often the voxel wise fMRI time series are averaged per brain region to compute the functional connectivity. For EEG/MEG, this can also be achieved following source estimation through an inverse model [185].

No gold standard pipeline has been agreed on within the neuroimaging community so far, and there is a large variety of possible steps to be included or not, which can affect the results, and consequently the input to virtual brain modeling. This variability was recently demonstrated in a meta-analysis, where 70 international independent teams analysed the same fMRI datasets with the pipeline of their choice. Interestingly, no two pipelines were identical, leading to sizeable variation in the statistical results obtained [186]. Similar studies have been conducted for tractography in diffusion weighted imaging datasets [187], [188], and another study on EEG data processing with the same intention is currently underway [189]. This highlights the fact that for well-grounded virtual brain modeling and inference, robust and well-tested image data preprocessing needs to be applied. To streamline the data preprocessing, different labs have packaged pipelines that take raw imaging data as input and give processed data as output. Each pipeline is differently adjustable and applicable to different quality of the input data. To name only a few examples: MICA pipe [190], fmriprep [191], nipreps (https://www.nipreps.org/), XCP-D pipe [192], MRtrix3 connectome [193], HCP minimal preprocessing pipeline [194],and a pipeline adjusted for virtual brain modeling on UK Biobank imaging data [195]. Computation time for preprocessing depends on the number of data modalities used, data resolution, specific processing steps involved, and possible manual intervention (e.g. in cases the algorithm fails). Intensive tasks include surface reconstruction, anatomical segmentation, tractography, and denoising. The processing of a

typical 3T MRI dataset (with T1w, diffusion, f-MRI) takes ∼12 h on a high-performance workstation. Some algorithms support parallel processing (CPU and GPU) for faster computation. While future algorithmic and computational advances may accelerate processing, increasing resolution and multimodal complexity could offset gains, making HPC infrastructure essential for cohort studies.

B. Simulation

The simulation of a VBT (e.g., given by Equation 5) is an initial value problem for the differential equations representing neural activity, along with any forward models required. In the most general case, the equations are partial, stochastic and time-delayed,

$$\frac{d}{dt}x_i(t) = f(x_i(t), X(t-\tau)) + z(x_i(t))\xi_i(t) \tag{7}$$

where x_i is the i'th state variable, f is the deterministic component of the model for the i'th variable, $X(t-\tau)$ are time delayed state variables, z is the diffusion component and ξ_i is a Brownian process. Note that the function f, which describes the dynamical properties of the system, encapsulates the local neural activity and the coupling function $G\sum_{j=1}^{N} \mathrm{w}_{ij}\mathcal{H}(\psi_i, \psi_j(t-\tau_{ij}))$ described in Equation 5. In practice, the partial derivatives are represented in a finite element fashion, thus not treated explicitly, additive diagonal Gaussian noise is used, time delays are fixed and follow a bounded unimodal distribution, and the equations are generally not stiff. While such equations can be solved with a variety of solvers, VBT solutions are usually obtained with an explicit stochastic Heun step, which is 2nd order in the deterministic component and 1st order in the stochastic component:

$$X_{t+1} = X_t + \frac{dt}{2}(f(X_t) + f(X_t + dtf(X_t) + Z_t)) + Z_t \tag{8}$$

where $Z_t = \sqrt{dt}g(X_t)dW_t$ and $dW_t \sim N(0,1)$.

In order to facilitate use by scientists, a Python package "The Virtual Brain (TVB)" has been written and maintained over the last decade, acting as a reference implementation [86], [196]. It is also available as open-source service on the cloud research platform EBRAINS (European Brain Research Infrastructures; ebrains.eu) [197]. The core library implements 29 different neural mass models, a handful of alternate numerical schemes, support for stimulation paradigms, along with several typical forward models for neuroimaging data, such as EEG, MEG, iEEG and fMRI. The fMRI solution is obtained either by solving the Balloon-Windkessel equations directly or via a linear approximation with a convolution. Some precalculation of so-called gain matrices for the EEG, MEG, iEEG forward models is provided, but we recommend using packages such as Brainstorm for this and importing the resulting gain matrix after for use in TVB.

The performance of Python, its NumPy array library and Numba JIT compiler in particular, enables pilot projects to design and test a specific model, but is insufficient for many "production" use cases, where the number of simulations to run for parameter sweep, simulation-based inference or Monte Carlo purposes is high. For these cases, tailored code is written either for CPU or GPU accelerators and supercomputing systems, usually involving adapting the layout of simulation work arrays for SIMD or SIMT parallelization, and high throughput schedulers such as Dask for distributing the work.

Several such implementations have been developed differing in the trade-offs between performance and productivity, as the translation of the mathematical formulation to the performance-oriented programming languages (such as C/C++) is a time-consuming and error-prone process. The hand-written single-purpose implementations of a given simulation configuration such as [198] provide good performance, but are limited in extensibility. Two main approaches have been adopted to address this productivity bottleneck of the domain scientists. First, the structure of the reference simulator is replicated in the software components of the performance-oriented implementation to reduce the learning curve for the users adapting it to their needs, such as the `TVB C++` [199] backend of TVB. Second, the simulation is defined in a high-level configuration format such as XML, and the performance-level code is then generated based on the user input, effectively decoupling the domain experts from the implementation-related aspects of the simulation. This approach, taken by the `RateML` [200] also simplifies targeting different computing devices and integration of performance optimizations relevant for specific use-cases, such as the high-resolution models [201].

C. Model-based Inference

Inference is the method through which conclusions, decisions, or predictions are derived from initial premises, evidence, or existing data [202]. Broadly speaking, in statistics, inference is the process of discovering general principles about a set based on limited samples drawn randomly [203]. In machine learning (ML), it usually refers to using a trained model to generate predictions on unseen data [204]. In some cases it refers to discovering a statistical generative model in order to generate new observations that resemble the original dataset (generative adversarial network, transformers). In the context of VBT, the inference process relies on connectome based network model, as the data generative process, to simulate brain activity. The aims of inference are now to discover the most likely causes (within the scope of the model) of some unseen data and to predict new outcomes under some intervention in the model. By further integrating subject specific multimodal structural and functional data, the VBT becomes unique and personalized parameters are estimated to maximize the model's predictive power, potentially informing clinical decision-making at the individual level. The evaluation of causal hypothesis also becomes possible *in silico*, in scenarios [205]–[207] where testing *in vivo*, such as electrode implantation or the removal of epileptogenic zones in epileptic patients, would be prohibitive [5], [7], [9].

When estimating the subject-specific parameters that best explain the data, the inference process recasts to model inversion. The set of parameters to be estimated often includes regional parameters, such as control (bifurcation) parameters, along with a global scaling factor that defines the role of the structural connectivity matrix in revealing network effects. To incorporate uncertainty in the estimation and integrate background knowledge, such as clinical information [208], [209], we use Bayesian inference, in which all model parameters are treated as random variables, and their values vary according to their underlying probability distributions [210]. Bayesian inference is a principled method that updates the probability of a hypothesis based on new evidence and prior knowledge. In other words, Bayes' rule combines and actualizes the prior information (background knowledge before seeing data) with the likelihood function (data-generating process) to form the posterior distribution (see Figure 6**A**). The posterior provides all the necessary information for evaluating accuracy and measuring out-of-sample predictive performance [211], [212]. Mathematically speaking, Bayes rule is defined as $p(\theta \mid y) = \frac{p(y|\theta)p(\theta)}{p(y)}$ where, $p(\theta \mid y)$ is the posterior distribution of parameters given the observed data, $p(y \mid \theta)$ is the likelihood of data given parameter, and $p(\theta)$ is the prior distribution. The denominator $p(y) = \int p(y \mid \theta)p(\theta)\, d\theta$ is the marginal likelihood or evidence, which normalizes the posterior distribution. Methods differ in providing either samples from the posterior, or a tractable function that approximates the posterior function. Dynamic Causal Modeling (DCM; [213]–[215]) is a well-established approach in neuroscience that relies on approximation techniques, such as the variational free

This article has been accepted for publication in IEEE Reviews in Biomedical Engineering. This is the author's version which has not been fully edited and content may change prior to final publication. Citation information: DOI 10.1109/RBME.2025.3562951

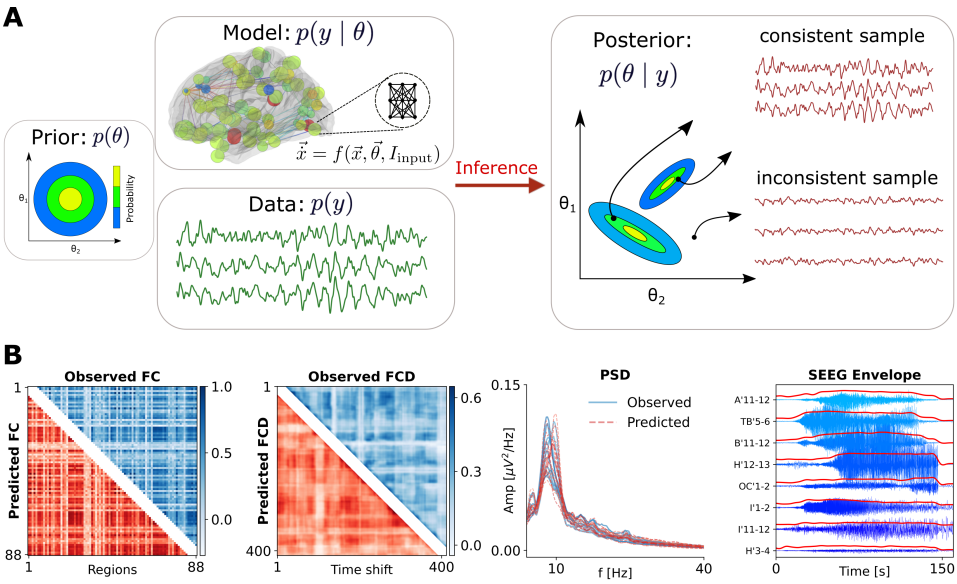

Fig. 6: **Bayesian inference in VBTs**. (**A**) Based on Bayes' theorem, background knowledge about control parameters in a VBT (expressed as a prior distribution, here in 2D), is combined with information from observed data (in the form of a likelihood function) to determine the posterior distribution. Markov chain Monte Carlo (MCMC) algorithms directly sample from the posterior distribution, while ML algorithms used in simulation-based inference (SBI) approach transforms a simple distribution (prior) into any complex target (posterior). Both methods inform us about degeneracy by providing all possible solutions in parameter space that best explain the data. (**B**) Examples of the observed and predicted data features in VBTs, such as functional connectivity (FC), functional connectivity dynamics (FCD), power spectral density (PSD), and SEEG envelope.

energy under the Laplace approximation (i.e., fixed-form Gaussian approximation to the posterior density), and it has been most widely applied to simple, linearly stable NMMs [216], [217]. VBTs typically use either Monte Carlo methods, or training deep neural networks to learn distributions (without the need to specify a variational family or rely on factorization, Gaussianity or conjugacy assumption), while also incorporating nonlinearity [218]–[220].

1) Markov chain Monte Carlo: The gold standard for unbiased sampling from the posterior distribution is a family of computational algorithms known as Markov chain Monte Carlo (MCMC; [221]). These algorithms evaluate consistency with empirical data through random simulations while preserving the correlation structure between parameters. Unlike point estimates such as maximum likelihood [222] or maximum a posteriori [223], Bayesian inference using MCMC provides the full posterior densities, allowing for a richer and more informative view of the parameter space, enhancing the quality of causal inference and decision-making. Adaptive and gradient-based MCMC sampling methods, such as the No-U-Turn Sampler [224], implemented in automatic probabilistic programming languages, like Stan [225], allow for accurate and efficient posterior estimation of parameters in VBTs. These techniques have been primarily opted for epilepsy as it involves complex dynamic brain activity patterns that require precise modeling [9], [144], [208], [218], [223], [226]. The particular geometry of a realized likelihood function or posterior density function depends on the chosen parameterization of the model configuration space [95]. We introduced intricate reparameterization for these models to facilitate convergence and accurately capture and recognize their configurations [218], [226]. Accurate and efficient estimation of parameters in such models is crucial for understanding and predicting seizure events [154], [227], [228], which has driven the development of advanced MCMC methods in this field.

2) Simulation-based inference: Due to the high dimensionality of the parameter space and the data, as well as the nonlinear dynamics involved in neural mass models, MCMC methods often become computationally prohibitive. Of the alternatives, probabilistic ML algorithms, such as simulation-based inference (SBI; [229], [230]), can efficiently estimate the posterior distribution of parameters given only the low-dimensional data features (see Figure 6**B**). Tailored to Bayes' rule, by using deep neural density estimators [231], [232] along with conducting random–but parallel simulations–, this class of probabilistic ML algorithms efficiently approximates the full posterior distribution of model parameters while reducing the computational challenges associated with calculating the likelihood function. Taking prior distribution $p(\vec{\theta})$ over the parameters $\vec{\theta}$, a limited number of N_{sim} simulations are generated for training step $\{(\vec{\theta}_i, \vec{y}_i)\}_{i=1}^{Nsim}$, where $\vec{\theta}_i \sim p(\vec{\theta})$ and $\vec{y}_i$ is the simulated data features given model parameters $\vec{\theta}_i$. After training step, we are able to efficiently estimate the approximated posterior $q_\phi(\vec{\theta} \mid \vec{y})$ with learnable parameters ϕ, so that for the observed data $\vec{y}_{obs}$: $q_\phi(\vec{\theta} \mid \vec{y}_{obs}) \simeq p(\vec{\theta} \mid \vec{y}_{obs})$. Importantly, SBI approach can be amortized at the subject-specific level, meaning that we do not need to retrain the model for new patient-specific data [219], [220]. As a result, we can retrieve the posterior distribution of parameters in an order of seconds. This approach has demonstrated its capability in revealing pathological causes in brain disorders such as epilepsy [219], multiple sclerosis [10], Alzheimer's disease [233], Parkinson's disease [11], as well as in healthy aging [15] and focal interventions [234]. Note that identifying the set of low-dimensional data features that are informative of the control parameters for each case study is the main challenge in effectively applying SBI approach. Moreover, as an approximation technique, SBI may slightly overestimate the uncertainty or the relationships between parameters due to the limited number of simulations and the use of low-dimensional features. Nevertheless, this can be mitigated by using time-delay embedding techniques for data augmentation [145], or restructuring the model configuration space–such as through hierarchical reparameterization–to facilitate more efficient exploration of the posterior distribution [220]. For model comparison, assessing model evidence using MCMC can be achieved by computing fully Bayesian information criteria, such as the widely applicable information criterion (WAIC) or Pareto-smoothed importance sampling (PSIS) leave-one-out cross-validation [211], [212]. These techniques, implemented in high-level tools such as Stan [225], leverage the full posterior distribution rather than a point estimate, allowing us to integrate prior information and efficiently estimate pointwise out-of-sample prediction accuracy with negligible computational overhead compared to the cost of model fitting [208], [209]. DCM, as implemented in popular toolboxes such as SPM [235], relies on minimizing free energy, which corresponds to the Kullback-Leibler divergence between the true and approximate posterior, minus the log evidence. This approach enables analytic solutions to the approximated posterior, eliminating the need for MCMC sampling and providing a variational bound on model ev-

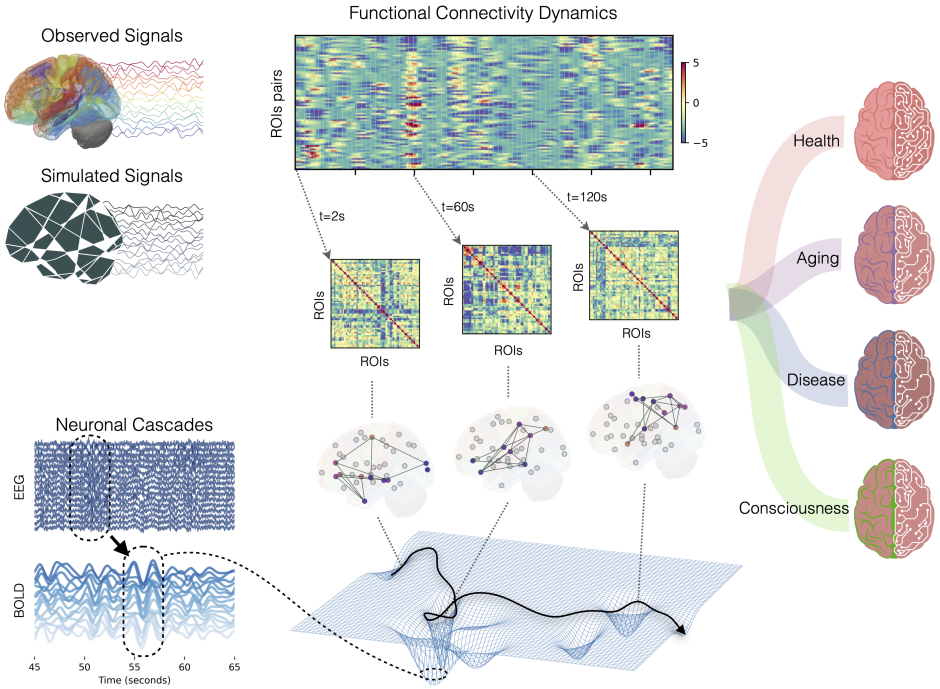

Fig. 7: **VBT of resting- and altered-states.** Brain activity at rest is characterized by the dynamic formation and disruption of strongly correlated communities. Such characteristic dynamics are naturally simulated in VBTs which are built on the connectomes. One way to represent FCD is via an edge-centric representation where, for each pair of ROIs, an edge co-activation time series is defined as the product between the standardized ROI-level signals. Averaging the co-activation signals (top raster plot) over time returns the Pearson's correlation for each edge i.e., the static FC. Thus, at each time, the configuration of edge co-activations corresponds to an instantaneous realization of the FC (see example matrices). In time, the system explores various network configurations, which can be understood in dynamical system jargon as attractors on the Neural Manifold. In terms of neural signals, these correspond to high-amplitude fluctuations, or *neuronal cascades*, involving large-scale brain subnetworks, which generally underlie a slowdown of the system's dynamics. FCD properties such as the variability of explored FC states (a.k.a., *fluidity*) or the richness of attractors dynamics (e.g., transition probabilities) are used as markers of health, disease, aging, and consciousness states.

idence for Bayesian model comparison [217], [236]. In this context, a thorough investigation of alternative approaches, such as SBI, is necessary for future studies.

V. Use cases of Virtual Brain Twin

In the following sections, we will demonstrate the use cases of the VBT, spanning the resting-state networks, healthy aging, multiple sclerosis, and epilepsy.

A. Resting state

Resting-state brain activity refers to the spontaneous neural processes that occur in the absence of specific tasks or external stimuli. Despite the absence of external demands, the brain's activity remains highly structured both spatially and temporally (see Figure 7). This organization is marked by non-trivial correlations across distant brain regions, forming coherent patterns of activity known as functional connectivity (FC; [237], [238]). Over time, these patterns exhibit dynamic behavior, as strongly correlated functional communities are continuously formed and disrupted, giving rise to functional connectivity dynamics (FCD; [49], [111], [239], [240]).

Resting-state activity, often considered the brain's default mode, serves as a baseline for cognitive processes [241]. Studying this baseline is clinically relevant, as alterations in resting-state FC have been linked to a range of neurological and psychiatric disorders, including Alzheimer's disease [242], [243], schizophrenia [244], and depression [245]. Additionally, resting-state network dynamics provide biomarkers for aging [15], [246], [247] and various states of consciousness [248], [249] (see Figure 7).

While dynamic resting-state networks provide valuable insights into both healthy and pathological brain function, it is crucial to understand how deviations from healthy activity occur to gain mechanistic insights for diagnosis and prognosis in pathological conditions. Reorganization of whole-brain FC can be triggered by several factors, such as neuromodulatory changes [250], alterations in tissue excitability [251], and modifications in brain-gut communication [252], among others. However, without generative models of brain dynamics, discerning these mechanisms is challenging due to the brain's emergent behavior, where studying individual parts in isolation cannot fully explain brain activity [253].

VBT offers a generative model that simulates brain dynamics resembling those measured empirically (Figure 7), enabling researchers to explore the underlying causes of FC reorganization. A key finding from these models is that a healthy brain operates near a critical-like regime [45], [111], [254]. Deviations from this regime are often observed during transitions in consciousness, aging, or disease states [255], with different parameter sets required to optimally capture such changes, ideally in a probabilistic manner (see subsection IV-C).

VBTs incorporate both the structural and dynamic aspects of brain function. Structural connectivity, which reflects the organization of white matter pathways, serves as the backbone for resting-state activity. Brain function simulated by VBTs relies on neural mass model equations (see subsection III-A). Realistic resting-state BOLD fMRI activity can be modeled using mean-field equations (see subsection III-A), with local parameters tuned close to instabilities, such as the Hopf model tuned near its bifurcation point [47]. However, while revealing the static dynamical core, this approach cannot identify its frequency-dependent aspects [62], which arise due to the interplay of the neuronal activity and the spatiotemporal profile of connectome's weights and time-delays [45], [61]. A more comprehensive view emerges with the neural masses tuned to bistability and driven by noise to generate local fluctuations between low and high firing rates, resembling patterns observed during slow-wave sleep, anesthesia, and quiet wakefulness [112]. These models replicate the multistable attractor dynamics observed in real brain data [111]. The activation patterns produced by VBTs occupy specific structural modules and closely reflect the transient co-activation patterns identified in resting-state fMRI studies [112], [256], [257].

Although co-activation events are rare and deviate from baseline activity–raising concerns about their potential as artifacts rather than genuine neural phenomena–they remain significant contributors to FC. Brain models demonstrate that these events can naturally occur and should not be dismissed as artifacts. Further evidence from

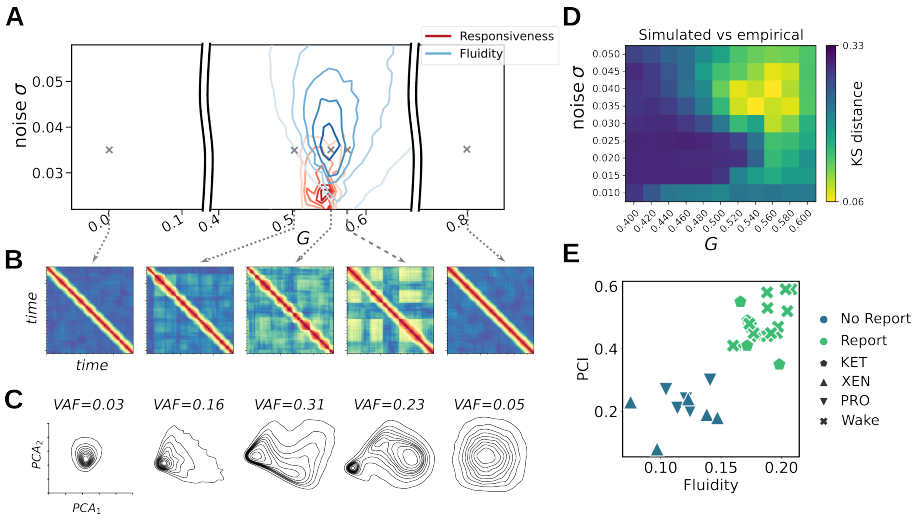

Fig. 8: Structural Connectivity shapes the manifold of resting state activity. (**A**) The VBT exhibits the fluid dynamics in a narrow range of connectivity scaling G, where the local dynamics and the network influence are balanced and the symmetry across the nodes is broken (blue). The system in the working point also exhibits the highest responsiveness when the driving noise is decreased (red). (**B**) The fluid dynamics as reflected in the FCD. (**C**) The dimensionality of the dynamics decreases in the working point, here shown in the projection of the model state variable time series into the first two PCA components, and assessed by the Variance Accounted For (VAF). (**D**) The simulated activity is most similar to the empirical data in the working point. (**E**) The prediction from the VBT regarding responsiveness was validated in the empirical data in subjects under anesthesia (Propofol, Xenon, Ketamine). The fluidity of the spontaneous activity performed as well as the perturbation complexity index in separating the cases of conscious report. Figure was adapted from our previous studies [44], [258].

fMRI data across species supports the idea that transient co-activation patterns may serve as foundational components of FCD [259]. These transient functionally connected communities align with the brain settling into specific attractor states, while transitions between patterns indicate metastable dynamics [260]–[263]. According to synergetics principles [19], [20], when the brain enters an attractor state, a few macroscopic variables dominate, reducing the complexity of the system. This reduction allows brain activity to be modeled as a low-dimensional flow in state space [49], [264], [265]. In the resting state, structural connectivity introduces asymmetry between brain nodes, creating characteristic flow on the manifold, that governs the evolution of brain activity (see Figure 8). This manifold represents the space of possible functional configurations constrained by structural connectivity [43], [44], [266], offering insights into brain dynamics like traveling waves and cascade effects. Importantly, the manifold naturally constrains the inference process, enabling the sampling and estimation of a nuanced relationship between personalized parameters and large-scale brain dynamics, which is crucial for understanding clinical outcomes.

VBTs have revealed the role of the neuromodulatory system in shaping brain dynamics by regulating the attractor landscape [250]. The organization of resting-state activity also underpins the brain's capacity to respond to external stimuli. Using VBT models, it has been shown that the complexity of stimulus-evoked responses, a reliable marker of consciousness [267], is tied to the same parametric regime in which spontaneous activity remains fluid i.e., flexibly switches between attractors [258] (see Figure 8). Fluidity measures applied to resting wakefulness versus anesthesia demonstrate a comparable ability to assess consciousness as traditional stimulation paradigms.

A striking example of the brain's interconnectedness is the widespread effect of local manipulations, such as focal lesions or optogenetic neuronal silencing, on resting-state brain organization [268]–[271]. VBTs confirm these findings, linking the observed reconfiguration to either structural lesions [272] or changes in local neuronal excitability [234]. In sum, VBTs offer powerful tools for formulating causal hypotheses and interpreting experimental data. By providing mechanistic insights into brain dynamics, they facilitate a deeper understanding of both healthy and pathological states of brain function.

B. Healthy aging

Aging of the brain is well described, both structurally and functionally [273], [274]. On the structural side, it leads to a substantial overall decrease in the number of streamlines [273], which mostly affects inter-hemispheric links that decrease with advancing age [15], [247]. On the functional side, applying graph theory metrics reveals age-related increases in between- and decreases in within-network resting-state FC [275]. However, FCD and higher order connectivities are more predictive of the brain age than the static FC [247], with age-related slowing down in FCD becoming evident when it is characterized as a random walk [246].

The observed patterns between structure and function have been statistically linked [276], including studies using TVB [277]. TVB was also used to demonstrate a link between the decrease in complexity of the brain's function with aging and its structural changes, represented as long-range pruning [278]. Similarly, demyelination and white matter atrophy, especially the decline of the long interhemispheric tracts, have been linked to changes in FCD and metaconectivity at the individual level, with a key role of dynamical compensation through the increased global coupling [247]. However, the individual-level variability of structure and function links to cognitive decline, has only recently been demonstrated [15].

Lavanga and colleagues built a Virtual Aging Brain (VAB; [15]) framework to infer the causal link between structural connectivity (SC) and functional architecture, and how this impacts the consequent cognitive decline in aging of the 649 healthy subjects in the range of 55-85 years from the 1000 Brains cohort [279], as schematically shown in Figure 9**A**. Based on the analysis of the personalized data and earlier works [247], interhemispheric degradation of SC was identified as a primary aging mechanism, Figure 9**B**. Testing this *in silico*, they reproduced the process of functional dedifferentiation during aging, Figure 9**C**. In particular, the study hypothesized that experimentally decreasing the interhemispheric SC (presented by the α mask parameter) would mimic a major mechanism of the structural aging process in the brain (i.e., "virtual aging"). This change would consequently be associated with reductions in the interhemispheric fluidity and the homotopic FC, as these two functional patterns demonstrate the highest sensitivity to aging. While setting up the working point of the virtual brains, the authors hypothesized that the brain attempts to maximize its fluidity (with FCD variance serving as a proxy) based on previous works that identified the FCD variance as an indicator of brain fluidity, which has been linked to cognitive

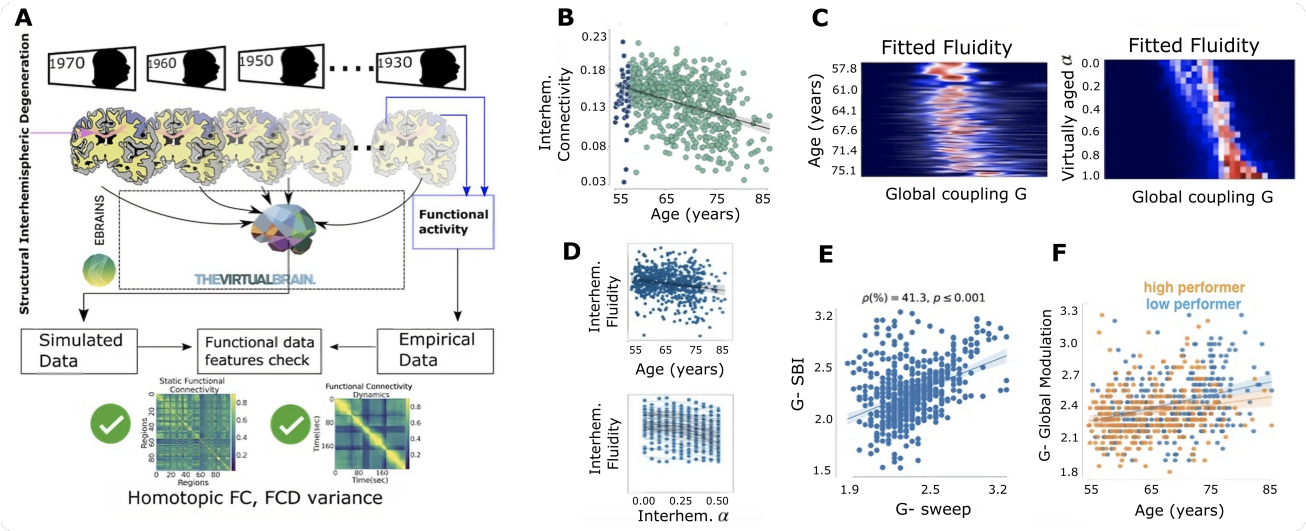

Fig. 9: **Virtual Aging Brain framework.** (**A**) Virtual brains are constructed using TVB simulator from a cohort of healthy subjects aged 55 to 85 years. The fMRI BOLD signals are simulated, and selected data features (homotopic functional connectivity and FCD variance) are compared with empirical data. (**B**) Interhemispheric SC decreases in the empirical data ($\rho = -0.453$, $p < 0.001$. The 50 youngest subjects, represented in blue, are later virtually aged. (**C**) Heatmap of the simulated FCD variance and its trend with age (left) and virtually aged through degraded interhemispheric connectivity (right). (**D**) Interhemispheric FCD variance as a metric of fluidity for the virtual subjects (top) and the virtually aged subjects (bottom). (**E**) The correlation between G modulation index obtained using Bayesian SBI and the G obtained by parameter sweep. (**F**) The aging G trend split by concept shifting: low performers (blue) and high performers (orange) (Fisher's-Z: $p = 0.046$, ρ corrected for sex and education). Figure was adapted from our previous study [15].

flexibility [112], [246], [280]. Based on this criterion, the VAB framework presented a significantly higher coupling between SC and FCD, indicated by a higher global network parameter G, with increased age, but also with stronger SC deterioration (corrected for sex and education), as shown in Figure 9**C**. Hence, this demonstrates that the global modulation, which was hypothesized to be linked with neuromodulation–particularly the dopaminergic processes [281]–plays a compensatory role in preserving cognitive capabilities, and it increases with age and with SC deterioration.

The Bayesian SBI [219], [220] also confirms the increase in SC neuromodulation with aging on an individual basis, as shown in Figure 9**D**, and retrieves global modulation with the same age-related declines in FC and FCD features. This provides a causal validation of the VAB pipeline and suggests that higher model evidence corresponds to increased G values with age, indicating a shift in the brain's optimal working point as it ages. Given that the age-related increase in SC-FC coupling is characterized by functional differentiation [282], the slightly stronger age-related increase observed in G in low-performing individuals, Figure 9**E**, might additionally reflect an acceleration of these processes. In addition to being applied in a task-free paradigm, this is direct evidence of scaffolding and dedifferentiation in aging [282], leading to adverse effects of cognitive decline as demonstrated within a subject-specific causal inference framework in a large cohort.

C. Multiple sclerosis

Multiple sclerosis (MS) is a chronic autoimmune disease of the central nervous system, affecting 2.8 million people worldwide in 2020 [283]. It results from immune attacks on the myelin sheath, impairing nerve signal transmission and causing motor and cognitive symptoms [283]. Clinical monitoring mainly relies on structural lesions to the myelin, but the total amount of lesions per se correlates poorly with clinical impairment (i.e., the clinical-radiological paradox [284]). Given the spatio-temporal heterogeneity of the lesions, and the growing availability of multimodal datasets [285], VBTs can help by building personalized models aimed at patient stratification [10] and, in the future, prediction of therapeutic outcome.

The disease alters large-scale brain connectivity, which VBTs can model [10], [17]. Predictive MS models have focused on therapy response, often using generalized linear models [286]. However, these do not directly explain patient-specific disabilities. The Virtual Multiple Sclerosis Patient (VMSP; [10]) offers a probabilistic approach linking symptoms to reduced conduction velocities, which are difficult to measure. While structural lesions are traditionally assessed via MRI to gauge disease progression and treatment response [287], VBTs infer conduction velocities more directly. MS patients show slower propagation of impulses, particularly in lesion-affected regions [285]. Changes in myelination disrupt brain region interactions, and time delays become key parameters reflecting disease impact. A multimodal study using MEG and tractography demonstrated that conduction delays could be inferred from MEG spectral properties [10].

To achieve this, the Jirsa-Haken equation was constrained to operate in the oscillatory regime, emphasizing the space-time structure of the connectome and time delays via signal propagation. To this end, we constrain the Jirsa-Haken equation, given by Equation 1, to operate the neural masses locally in the oscillatory regime. In such reduced form, this can be written using Stuart-Landau oscillators (known as the normal form of a Hopf bifurcation, see Table I) coupled through to the empirical patient-specific connectomes as in:

$$\begin{aligned}\dot{Z}_j &= Z_j(a + i\omega_j - |Z_j|^2) + G\sum_{k=1}^{N} \mathrm{SC}_{jk}[Z_k(t-\tau_{jk}) - Z_j(t)] \\ &\quad + \sigma(\eta_{j1} + i\eta_{j2}),\end{aligned} \tag{9}$$

where Z is a complex variable, and $\mathrm{Re}[Z(t)]$ is the corresponding time series. Each region has a natural frequency of 40 Hz ($\omega_j = \omega_0 = 2\pi \cdot 40\ rad/s$). Note that coupling between regions (with strength of SC, and scaled by G) accounts for finite conduction times, which are estimated by dividing the Euclidean distances between nodes by an average conduction velocity $\tau_{jk} = d_{jk}/\nu$ (see Equation 6, and Equation 5).

Low-dimensional data representations captured the power spectra expected under specific delays (Figure 10**A**, **B**), effectively model-

This article has been accepted for publication in IEEE Reviews in Biomedical Engineering. This is the author's version which has not been fully edited and content may change prior to final publication. Citation information: DOI 10.1109/RBME.2025.3562951

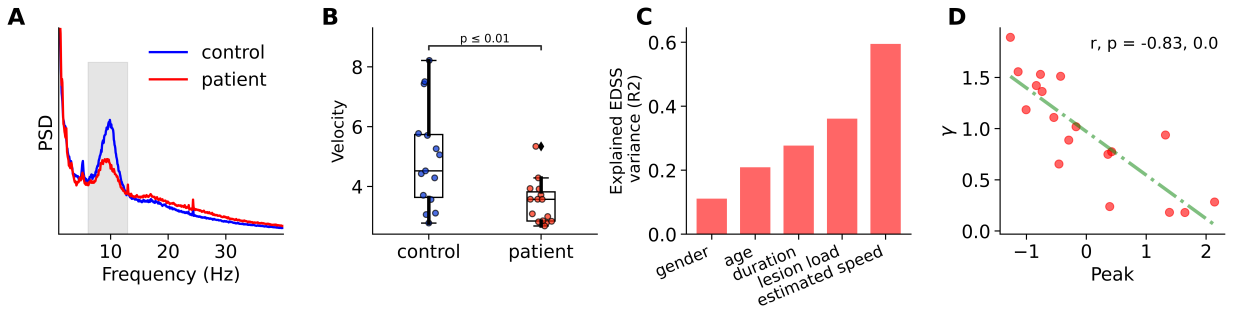

Fig. 10: **Virtual Multiple Sclerosis framework.** The individualized DTI and empirical MEG data were integrated into personalized virtual brain models to estimate conduction velocities in MS patients and controls using Bayesian inference. (**A**) Median power spectral density (PSD) plotted for controls (blue) and MS patients (red). Shaded region represents the alpha band (8–13 Hz). (**B**) The inferred velocity parameter significantly decreases in the control group relative to the patient group. (**C**) Variance explained by the additive model including five variables (i.e., gender, age, disease duration, lesion load, and estimated speed). Adding the estimated conduction velocities significantly increased the predictive power. (**D**) Correlation between inferred parameter γ (translating lesion into edge-specific conduction delays) and the amplitude of alpha-peak in MEG recordings. Figure was generated using methods and data from our previous study [10], [17].

ing synchronization dynamics [10], [17]. Weak coupling and large delays prevented synchronization, while strong coupling induced slower, lower-amplitude oscillations [61], [288]. Assuming intermediate coupling, spectral summary statistics trained deep neural density estimators within simulation-based inference (subsection IV-C). The inferred individual average delays predicted clinical disability (Figure 10**C**).

As mentioned, a key MS challenge is patient-specific damage variability. Not all brain connections are affected, and lesion locations differ. Relying on average delays loses crucial lesion topography information, while inferring delays for thousands of edges is computationally prohibitive due to high dimensionality and degeneracy. A novel approach addressed this by linearly linking conduction delays to white matter tract damage [17]. This function, dependent on a single control parameter, translates lesion intensity into edge-specific conduction delays across all lesioned edges, shifting power spectra (Figure 10**D**). Parameters estimated via neural density estimators were predictive of clinical disability [10], [17]. This study marks an important step in tailoring VBTs for MS, showcasing how models can provide a framework to integrate personalized multimodal data into a coherent framework, both form the mathematical and pathophysiological standpoint.

D. Epilepsy

Epilepsy affects around 50 million people worldwide and can lead to long-term disability. The burden of epilepsy arises from several factors, including a high prevalence of drug resistance (around 30% of cases) and comorbidities such as depression and anxiety [5]. Seizure generation and propagation involve large-scale neuronal networks, and the complex spatiotemporal dynamics in recorded data cannot be easily explained by the traditional model of a single seizure focus triggering activity that spreads to non-epileptogenic brain regions [121], [122].

The first practical use case of VBTs was developed for epilepsy, known as the Virtual Epileptic Patient (VEP; [8]). The initial concept for constructing personalized whole-brain network models in epilepsy was introduced previously [8], [218], where the key building blocks were detailed. This first application focused on estimating the epileptogenic zone networks (EZN). The VEP workflow for estimating EZNs was evaluated using data from 53 patients with drug-resistant focal epilepsy [9], [289]. VEP is currently being evaluated in an ongoing clinical trial (EPINOV NCT03643016) with an enrollment of 356 prospective patients. The VEP is now also being used to predict surgical outcomes through virtual surgeries [9] and to explore electrical stimulation techniques such as SEEG and temporal interference stimulation [290].

Here, we briefly describe the modules of the VEP workflow, which can be considered standard construction patterns for VBTs in both healthy and diseased brains. The VEP extracts individual brain anatomy from T1-weighted MRI (T1-MRI) and defines 162 brain regions according to the VEP atlas [291]. Tractography is performed on diffusion-weighted MRI (DW-MRI) data to estimate the length and density of white matter tracts (subsection IV-A). These tracts are then grouped according to the regions defined by the atlas, allowing for the derivation of a structural connectivity matrix that specifies the connection strength between brain regions. The post-SEEG implantation CT scan is used to determine the exact locations of the SEEG electrodes and to construct the source-to-sensor map using the gain matrix (subsection III-C). The gain matrix maps the simulated neural source activity to the corresponding SEEG signals. Neural mass models at each source location are connected via the connectivity matrix, and neural source activity is then simulated (subsection III-A). Finally, Bayesian inference methods are employed to estimate patient-specific parameters of the model based on features extracted from SEEG signals and priors derived from additional knowledge, such as SEEG data analysis or clinical hypotheses (subsection IV-C). The output is the suggested EZN, which can be represented in a distribution table and a heatmap overlaid on the T1-MRI data.

Figure 11 presents a patient example to illustrate how the VEP works. This 29-year-old right-handed female patient was initially diagnosed with left frontal epilepsy (Figure 11**A**, **B**). Adaptive optimization and MCMC sampling algorithms were used to estimate the key parameters of the VEP models based on the data features from SEEG seizure recordings. These key parameters, including the excitability of each region and the global connectivity coupling, determined the epileptogenicity values for each region. The VEP identified the EZN from the posterior distribution of these epileptogenicity values (Figure 11**C**). Based on the clinical hypothesis, the EZN was thought to involve the left insula gyri brevi and the left orbitofrontal cortex (Figure 11**D**, shown in yellow). The patient underwent resective surgery targeting the clinically defined EZN, which resulted in a reduction in seizure frequency but did not achieve seizure freedom. According to the VEP, the EZN included not only the left insula gyri brevi and the left orbitofrontal cortex but also the left inferior frontal sulcus (Figure 11**D**, shown in red). The left inferior frontal sulcus was an additional region identified by the VEP. Based on this finding, and after reviewing all related patient data, the patient underwent a second surgery. The patient has been seizure-free

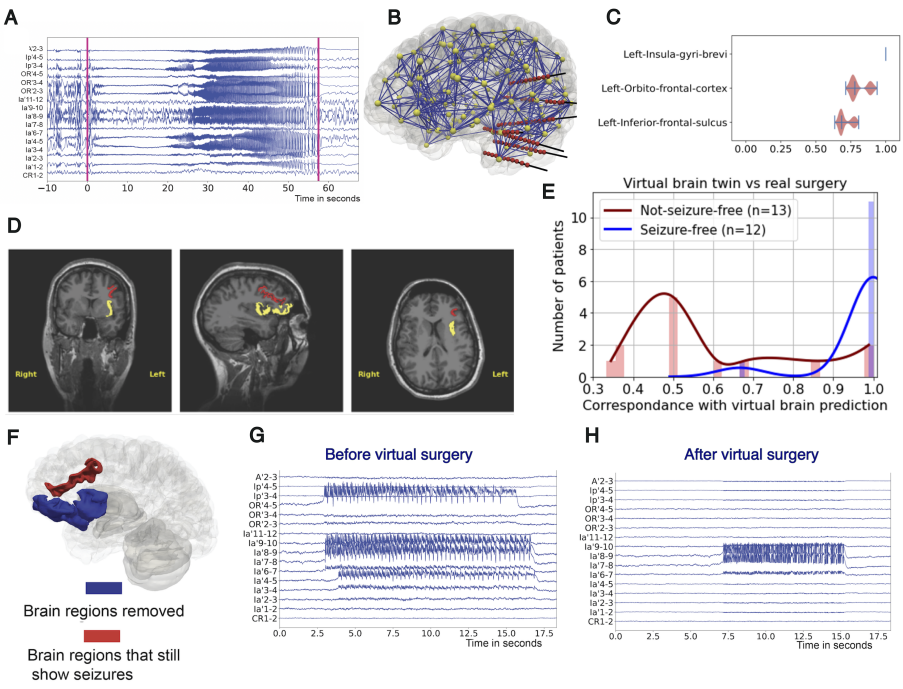

Fig. 11: **Virtual Epileptic Patient framework.** (**A**) Selected SEEG recordings from a 29-year-old female patient. (**B**) Personalized whole-brain models: brain region nodes are shown in yellow, connectivity links in blue, and SEEG electrodes in red. (**C**) Posterior distribution of the EV (where higher values indicate a higher probability of seizure) for three selected regions obtained from the MCMC sampling pipeline. (**D**) Heatmap of regions identified exclusively by VEP (red) and overlapping regions with the clinical hypothesis (yellow), displayed on a preoperative T1-MRI. (**E**) Precision of VEP compared to postoperative MRI in 12 seizure-free patients and 13 non–seizure-free patients. (**F**) The left insula gyri brevi and left orbitofrontal cortex (blue) were virtually resected, while the left inferior frontal sulcus (red) continued to show seizure activity. (**G**) Selected simulated SEEG time series using the estimated EZN by VEP pipeline. (**H**) Selected simulated SEEG time series after virtual surgery. Adapted from our previous study [9].

for over two years.

The VEP workflow was retrospectively evaluated using data from 53 patients with drug-resistant focal epilepsy [9]. VEPs accurately reproduced the clinically defined EZNs with a precision of 0.6, where the physical distance between epileptogenic regions identified by VEP and the clinically defined EZNs was small [9]. When comparing the VEP results with the resected brain regions, precision was used as a performance metric, highlighting the importance of minimizing false positives. In seizure-free patients, it is reasonable to assume that the EZN was completely removed, and thus any false-positive estimate is likely to be truly outside the EZN. Conversely, in non–seizure-free patients, a false-positive estimate is likely to correspond to non-resected epileptogenic regions, which may contribute to the persistence of seizures. The VEP demonstrated a very high precision (mean, 0.972) for seizure-free patients (Figure 11**E**). In contrast, the VEP results for the non–seizure-free group showed a significant decrease in precision (mean: 0.593) [5], [9], suggesting that there may be potential to better exploit the predictive power of the VEP. It should be noted that, in some patients, the very large extent of resection also contributed to the high precision value to some degree.

VBTs enable the simulation of brain activity data under various conditions, such as different stimulation protocols, seizure onset scenarios, or interictal states. As shown in Figure 12, once the VBT is constructed from the patient's specific data, we can simulate brain activity and map it to SEEG signals, enabling a direct comparison with the patient's empirical SEEG signals. The simulated signals from the VBT, generated with subject-specific control parameters, can provide a ground truth for detailed data analysis studies, such as evaluating algorithms and methods for estimating the EZNs [9] or testing EEG and MEG source localization algorithms [293], [294].

Another practical use of VBTs is providing virtual surgery results for patients with drug-resistant epilepsy. Epilepsy surgery is the only curative option to stop seizures in individuals with drug-resistant focal epilepsy [5]. However, the failure of surgery can result from several factors inherent to epilepsy (e.g., involvement of eloquent cortices or extended networks), the surgical procedure (e.g., insufficient resection), or SEEG assessment (e.g., inadequate investigation, sampling limitations, or challenges in interpreting findings). A follow-up SEEG assessment after unsuccessful epilepsy surgery may reveal an additional epileptogenic area near the original zone or in distant regions. The VBT has the potential to improve postsurgical outcomes by enhancing the prediction of the extent of the epileptogenic zone, the behavior of non-operated regions, and the potential effectiveness of surgery [9], [295], [296]. For instance, VBT can provide information on brain regions not sampled by SEEG and be used for model testing under conditions different from those used in the model's construction, such as simulating different clinical hypotheses for ictal and interictal states and testing surgical strategies (Figure 11**F**-**H**). These applications highlight a key advantage of VBTs over model-free approaches, which are limited to the regions explored by SEEG [5].

E. Parkinson's disease

In Parkinson's disease, brain-wide communication is disrupted [297], [298]. Interventions like L-Dopa and deep brain stimulation (DBS) induce therapeutic "desynchronization" of neural activities [299], [300]. Computational modeling has simulated these effects [301]–[305]. However, a key challenge remains incorporating dopamine into models, which was recently tackled [84], correctly predicting the effects of administration of L-Dopa on the large-scale activities at the individual level [11].

VI. Outlook and Discussion

Virtual Brain Twins (VBTs) offer a powerful tool for understanding and treating neurological disorders. By integrating structural and functional data, VBTs simulate brain dynamics, enabling Bayesian inference of personalized parameters and causal mechanisms. They allow *in silico* testing of interventions when *in vivo* experiments are not feasible (e.g., epilepsy), supporting more precise treatments. Clinical fields of application are rapidly expanding.

Mechanistic models simulate brain network reorganization post-infarct for stroke recovery, predicting how rehabilitation strategies influence functional recovery. Brain models quantify lesion impact on dynamics, aiding personalized rehabilitation [306]. Virtual stroke patient cohorts enable *in silico* testing of therapies and medical devices

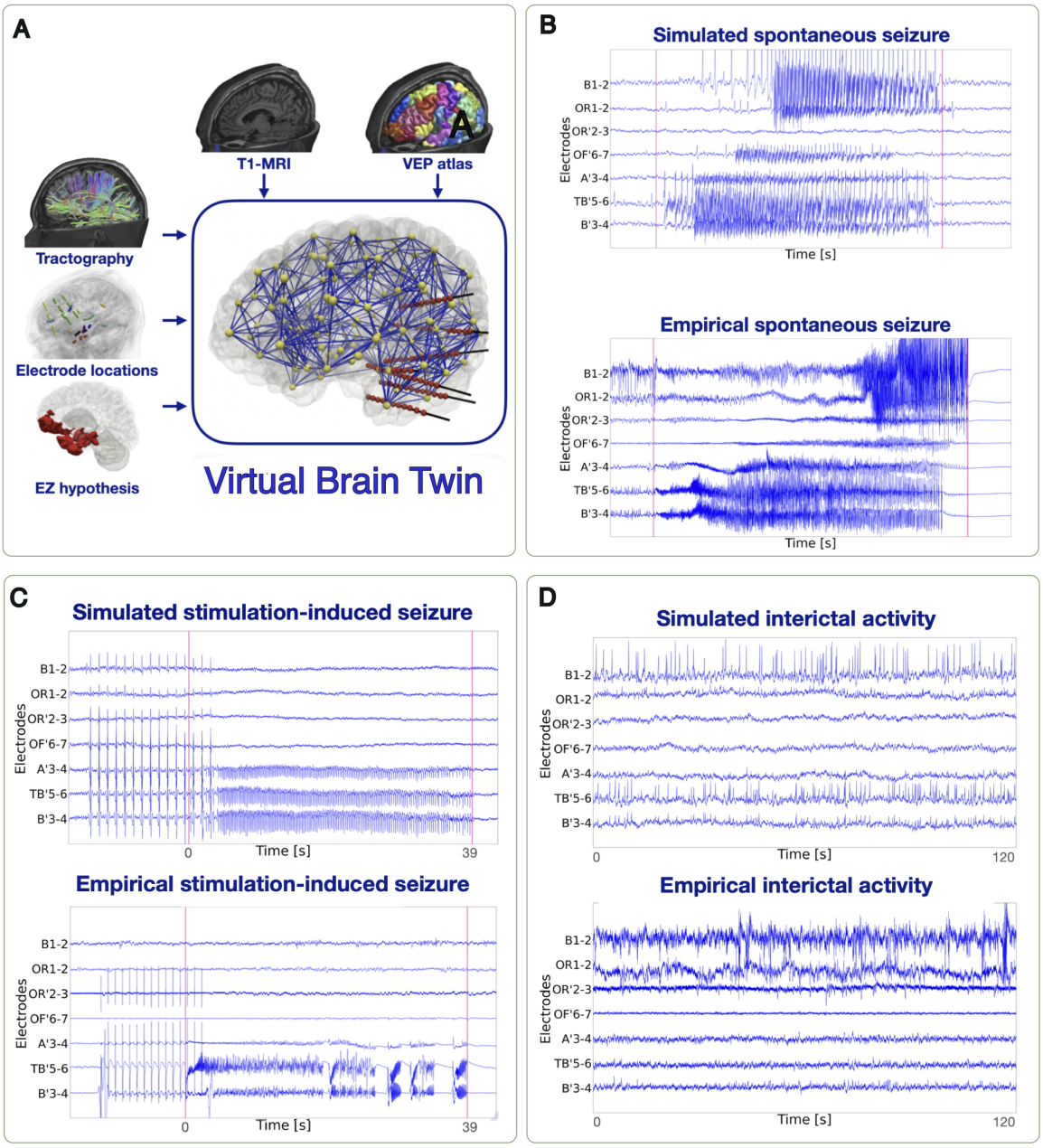

Fig. 12: **SEEG time series in the VBT of epilepsy.** (**A**) The VBT was constructed using the patient's specific data. For the same patient, the time series of simulated SEEG signals (top) and empirical SEEG signals (bottom) are shown for three different conditions: (**B**) Spontaneous seizures, (**C**) Stimulation-induced seizures, and (**D**) Interictal activity. Figure was adapted from [292].

[13]. In neuropsychiatric disorders, computational models address the lack of mechanistic understanding, bridging microscopic mechanisms to symptoms [307], [308]. This approach remains underexplored but has the potential to improve diagnosis and treatment. VBT applications have identified biomarkers across paradigms [10], [11], [258]. A TMS-EEG protocol associated with consciousness levels [267] was simulated in a VBT, linking brain dynamics to the perturbational complexity index (PCI). Simulating spontaneous activity in the same model validated PCI's role in responsiveness, opening new avenues for hypothesis testing through *in silico* experiments. Computational models can advance brain stimulation techniques, including transcranial magnetic stimulation (TMS), deep brain stimulation (DBS), and temporal interference (TI). These models predict stimulation effects, optimizing intervention parameters [309]–[311]. TI, a non-invasive technique, applies intersecting high-frequency currents to modulate neural activity [312]–[314]. However, technical challenges remain in generating precise stimulation patterns [315]. Control theory conceptualizes the brain as a dynamical system influenced by prior states, connectivity, and perturbations [316], [317]. Recent work demonstrated that brain stimulation can improve network estimations in neurodegenerative conditions by increasing transition probabilities between hidden states [220]. VBT might help the development of these approaches, improving the lives of people with PD, epilepsy, and depression, and enabling personalized interventions with fewer side effects.

Inference in VBTs is typically conducted via MCMC sampling [144], [218], [226] or SBI [219], [220]. Computational cost depends on model complexity and data resolution. MCMC sampling from SEEG data took ∼7-15 hours, while SBI achieved a 14x speedup. Optimization-based methods achieve lower computational cost by

compromising on the full posterior calculation [223], [227]. Note that MCMC is amenable to "embarrassingly parallel", as different chains can be run on different cores [208]. However, using SBI, the simulations can be executed in parallel, significantly reducing total runtime depending on available computational resources. Importantly, the training process in SBI is fast, typically requiring just a few min, while generating samples from the posterior takes only sec, demonstrating its efficiency [220], [230]. Moreover, SBI is amortized, allowing immediate application to new recordings without the need for retraining, making it highly scalable for real-time inference [219]. The open-source `VBI` toolkit [318] facilitates efficient probabilistic inference across neuroimaging modalities. ML techniques, such as normalizing flows [219], [319], variational autoencoders [146], [320], and neural ODEs [142], [145], are effective for probabilistic inference and neural system modeling, with potential applications in diagnosis and treatment planning [7], [10], [15], [233], [234]. These generative ML models are expected to enable precise, automatic inference of brain diseases from large, multimodal data in the near future.

Computational models play a critical role in the design and testing of neuromorphic devices such as brain-computer interfaces (BCIs), enabling researchers to simulate neural processes and predict how these interfaces will interact with the brain. By using these models, developers can explore different design options, optimize algorithms, and identify potential issues before implementing BCIs in real-world scenarios. For example, it has been proposed that brain models might be deployed to test causal relationships among variables of interests [321]. Furthermore, brain models can be used to optimize the design of the interfaces themselves. As an example, brain models might be used to provide a parsimonious description of the dynamics, which in turn can help define the most suitable decoders [322]. All in all, computational models might reduce the need for extensive animal or human testing, accelerate the development process, and enhance the safety and effectiveness of BCIs, paving the way for more advanced and personalized neurotechnologies.

Alternative approaches to VBTs offer different methodologies to achieve comparable outputs. As an example, AI-based predictive models and pharmacogenomics analyze genetic and imaging data to tailor therapies [323], though they often lack mechanistic insights. Computer-assisted surgical planning [324] and preoperative fMRI/PET mapping assist in epilepsy surgery but do not simulate post-surgical outcomes. However, they may serve as complementary tools for SEEG implantation planning. Connectomics-based approaches integrate multimodal brain data to study network disruptions [325], yet they do not provide individualized simulations. In disease progression modeling, deep learning applied to neuroimaging tracks neurodegeneration [326], [327] and predicts disease evolution, but it lacks causal brain network integration. For testing mechanisms and therapies, large-scale biophysical neural models (using toolkits such as GENESIS [328], NEURON [329], NEST [330], BRIAN [331], BMTK [332], BDtoolbox [333], and SRNN-Brain-Modelling-Toolbox [334]) offer valuable insights. However, they are not personalized and lack integration with probabilistic inference algorithms. Nevertheless, they can provide mechanistic constraints to neural mass models. The popular DCM is furnished with effective connectivity using fixed variational schemes (e.g., Laplace approximation), whereas VBT focuses on personalized structural connectivity and bifurcation parameters (using MCMC and SBI methods). While these approaches contribute valuable insights and may complement VBTs, none fully replicate their unique combination of personalization, dynamical whole-brain modeling, and mechanistic interpretability. Additionally, VBTs incorporate probabilistic machine learning algorithms (e.g., using `VBI` toolkit [318]) to rigorously quantify uncertainty and improve hypothesis testing. These features make VBTs particularly powerful for both neuroscience research and clinical applications. Nevertheless, VBT has limitations. Model-based approaches are typically computationally expensive and parameter-sensitive, posing challenges for practical use in clinical routine. Furthermore, VBTs do not currently account for long time scales. For instance, seizure patterns often exhibit irregular daily to monthly fluctuations, which are not modeled in current VBT implementations. Additionally, neural mass modeling simplifies brain dynamics, potentially limiting the granularity of simulated activity. A promising solution is to apply model inversion on the high-resolution data from next-generation neural field models to improve spatial and temporal precision. For any inference method, large datasets remain a big challenge.

In conclusion, VBTs represent a powerful tool for the prediction of therapeutic outcomes and the design of new devices that interact with the brain. Furthermore, these models offer detailed insights into the biological underpinnings of brain function and dysfunction.

ACKNOWLEDGEMENTS

This research has received funding from EU's Horizon 2020 Framework Programme for Research and Innovation under the Specific Grant Agreements No. 101147319 (EBRAINS 2.0 Project), No. 101137289 (Virtual Brain Twin Project), and government grant managed by the Agence Nationale de la Recherche reference ANR-22-PESN-0012 (France 2030 program). The funders had no role in study design, data collection and analysis, decision to publish, or preparation of the manuscript.

AUTHOR CONTRIBUTIONS

All authors contributed to the writing, editing, visualization, data analysis, and interpretation of the results, as well as to the overall conceptualization and development of the manuscript.

CONFLICT OF INTEREST STATEMENT

None declared.

REFERENCES

[1] N. J. Schork, "Personalized medicine: time for one-person trials," *Nature*, vol. 520, no. 7549, pp. 609–611, 2015.
[2] J. J. Tao *et al.*, "Basket studies: redefining clinical trials in the era of genome-driven oncology," *Annual review of medicine*, vol. 69, no. 1, pp. 319–331, 2018.
[3] O. Sporns, *Networks of the Brain*. MIT press, 2016.
[4] M. Breakspear, "Dynamic models of large-scale brain activity," *Nature neuroscience*, vol. 20, no. 3, pp. 340–352, 2017.
[5] V. Jirsa *et al.*, "Personalised virtual brain models in epilepsy," *The Lancet Neurology*, 3 2023.
[6] K. Amunts *et al.*, "The coming decade of digital brain research: A vision for neuroscience at the intersection of technology and computing," *Imaging Neuroscience*, vol. 2, pp. 1–35, 2024.
[7] H. E. Wang *et al.*, "Virtual brain twins: from basic neuroscience to clinical use," *National Science Review*, vol. 11, no. 5, p. nwae079, 2024.
[8] V. K. Jirsa *et al.*, "The virtual epileptic patient: individualized whole-brain models of epilepsy spread," *Neuroimage*, vol. 145, pp. 377–388, 2017.
[9] H. E. Wang *et al.*, "Delineating epileptogenic networks using brain imaging data and personalized modeling in drug-resistant epilepsy," *Science Translational Medicine*, vol. 15, 1 2023.
[10] P. Sorrentino *et al.*, "The virtual multiple sclerosis patient," *Iscience*, vol. 27, no. 7, 2024.
[11] M. Angiolelli *et al.*, "The virtual parkinsonian patient," *medRxiv*, pp. 2024–07, 2024.
[12] R. Laubenbacher *et al.*, "Digital twins in medicine," *Nature Computational Science*, vol. 4, no. 3, pp. 184–191, 2024.
[13] C. Miller *et al.*, "In silico trials for treatment of acute ischemic stroke: design and implementation," *Computers in biology and medicine*, vol. 137, p. 104802, 2021.

[14] D. L. Kurtin *et al.*, "Moving from phenomenological to predictive modelling: Progress and pitfalls of modelling brain stimulation in-silico," *Neuroimage*, vol. 272, p. 120042, 2023.

[15] M. Lavanga *et al.*, "The virtual aging brain: Causal inference supports interhemispheric dedifferentiation in healthy aging," *NeuroImage*, vol. 283, p. 120403, 2023.

[16] L. Stefanovski *et al.*, "Bridging scales in alzheimer's disease: biological framework for brain simulation with the virtual brain," *Frontiers in Neuroinformatics*, vol. 15, p. 630172, 2021.

[17] C. Mazzara *et al.*, "Mapping brain lesions to conduction delays: the next step for personalized brain models in multiple sclerosis.," *medRxiv*, pp. 2024–07, 2024.

[18] J. M. Shine *et al.*, "Computational models link cellular mechanisms of neuromodulation to large-scale neural dynamics," *Nature neuroscience*, vol. 24, no. 6, pp. 765–776, 2021.

[19] H. Haken, "Synergetics," *Physics Bulletin*, vol. 28, no. 9, p. 412, 1977.

[20] H. Haken, *Principles of brain functioning: a synergetic approach to brain activity, behavior and cognition*, vol. 67. Springer Science & Business Media, 2013.

[21] P. L. Nunez, "The brain wave equation: a model for the eeg," *Mathematical Biosciences*, vol. 21, no. 3-4, pp. 279–297, 1974.

[22] P. Nunez, *Electrical Fields of the Brain*. Oxford University Press, Oxford, 1981.

[23] P. L. Nunez and R. Srinivasan, *Electric fields of the brain: the neurophysics of EEG*. Oxford University Press, USA, 2006.

[24] H. R. Wilson and J. D. Cowan, "Excitatory and inhibitory interactions in localized populations of model neurons," *Biophysical journal*, vol. 12, no. 1, pp. 1–24, 1972.

[25] S.-i. Amari, "Dynamics of pattern formation in lateral-inhibition type neural fields," *Biological cybernetics*, vol. 27, no. 2, pp. 77–87, 1977.

[26] B. J. Cook *et al.*, "Neural field models: A mathematical overview and unifying framework," *Mathematical Neuroscience and Applications*, vol. 2, 2022.

[27] P. L. Nunez, "Neocortical dynamics and human eeg rhythms," *(No Title)*, 1995.

[28] V. Jirsa and H. Haken, "Field theory of electromagnetic brain activity," *Phys. Rev. Lett.*, vol. 77, no. 5, pp. 960–963, 1996.

[29] V. K. Jirsa and H. Haken, "A derivation of a macroscopic field theory of the brain from the quasi-microscopic neural dynamics," *Physica D: Nonlinear Phenomena*, vol. 99, no. 4, pp. 503–526, 1997.

[30] W. J. Freeman III, "Waves, pulses, and the theory of neural masses," *Progress in theoretical biology*, vol. 2, no. 1, pp. 1–10, 1972.

[31] W. J. Freeman, "Simulation of chaotic eeg patterns with a dynamic model of the olfactory system," *Biological cybernetics*, vol. 56, no. 2, pp. 139–150, 1987.

[32] V. K. Jirsa and J. S. Kelso, "Spatiotemporal pattern formation in neural systems with heterogeneous connection topologies," *Physical Review E*, vol. 62, no. 6, p. 8462, 2000.

[33] V. Jirsa *et al.*, "Spatiotemporal forward solution of the eeg and meg using network modeling," *IEEE transactions on medical imaging*, vol. 21, no. 5, pp. 493–504, 2002.

[34] V. K. Jirsa, "Neural field dynamics with local and global connectivity and time delay," *Philosophical Transactions of the Royal Society A: Mathematical, Physical and Engineering Sciences*, vol. 367, pp. 1131–1143, 3 2009.

[35] P. A. Robinson *et al.*, "Propagation and stability of waves of electrical activity in the cerebral cortex," *Physical Review E*, vol. 56, no. 1, p. 826, 1997.

[36] P. A. Robinson *et al.*, "Prediction of electroencephalographic spectra from neurophysiology," *Physical Review E*, vol. 63, no. 2, p. 021903, 2001.

[37] C. J. Rennie *et al.*, "Unified neurophysical model of eeg spectra and evoked potentials," *Biological cybernetics*, vol. 86, no. 6, pp. 457–471, 2002.

[38] F. Lopes da Silva *et al.*, "Model of brain rhythmic activity: the alpha-rhythm of the thalamus," *Kybernetik*, vol. 15, pp. 27–37, 1974.

[39] F. Freyer *et al.*, "Biophysical mechanisms of multistability in resting-state cortical rhythms," *Journal of Neuroscience*, vol. 31, no. 17, pp. 6353–6361, 2011.

[40] R. Hindriks and M. J. van Putten, "Thalamo-cortical mechanisms underlying changes in amplitude and frequency of human alpha oscillations," *Neuroimage*, vol. 70, pp. 150–163, 2013.

[41] M. Hashemi *et al.*, "How the cortico-thalamic feedback affects the eeg power spectrum over frontal and occipital regions during propofol-induced sedation," *Journal of Computational Neuroscience*, vol. 39, pp. 155–179, 2015.

[42] V. Jirsa and H. Sheheitli, "Entropy, free energy, symmetry and dynamics in the brain," *Journal of Physics: Complexity*, vol. 3, no. 1, p. 015007, 2022.

[43] A. S. Pillai and V. K. Jirsa, "Symmetry breaking in space-time hierarchies shapes brain dynamics and behavior," *Neuron*, vol. 94, no. 5, pp. 1010–1026, 2017.

[44] J. Fousek *et al.*, "Symmetry breaking organizes the brain's resting state manifold," *bioRxiv*, pp. 2022–01, 2022.

[45] A. Ghosh *et al.*, "Noise during rest enables the exploration of the brain's dynamic repertoire," *PLoS Comput. Biol.*, vol. 4, p. e1000196, Oct. 2008.

[46] M. Breakspear *et al.*, "Generative models of cortical oscillations: neurobiological implications of the kuramoto model," *Frontiers in human neuroscience*, vol. 4, p. 190, 2010.

[47] G. Deco *et al.*, "The dynamics of resting fluctuations in the brain: metastability and its dynamical cortical core," *Scientific reports*, vol. 7, no. 1, p. 3095, 2017.

[48] G. Deco *et al.*, "Key role of coupling, delay, and noise in resting brain fluctuations," *Proceedings of the National Academy of Sciences of the United States of America*, vol. 106, no. 25, pp. 10302–10307, 2009.

[49] G. Deco *et al.*, "Emerging concepts for the dynamical organization of resting-state activity in the brain," *Nat. Rev. Neurosci.*, vol. 12, no. 1, pp. 43–56, 2011.

[50] P. A. Robinson *et al.*, "Eigenmodes of brain activity: Neural field theory predictions and comparison with experiment," *NeuroImage*, vol. 142, pp. 79–98, 2016.

[51] N. C. Gabay and P. Robinson, "Cortical geometry as a determinant of brain activity eigenmodes: Neural field analysis," *Physical Review E*, vol. 96, no. 3, p. 032413, 2017.

[52] O. Sporns *et al.*, "The human connectome: a structural description of the human brain," *PLoS computational biology*, vol. 1, no. 4, p. e42, 2005.

[53] C. J. Honey *et al.*, "Predicting human resting-state functional connectivity from structural connectivity," *Proceedings of the National Academy of Sciences*, vol. 106, no. 6, pp. 2035–2040, 2009.

[54] M. Rubinov and O. Sporns, "Complex network measures of brain connectivity: uses and interpretations," *Neuroimage*, vol. 52, no. 3, pp. 1059–1069, 2010.

[55] D. S. Bassett and O. Sporns, "Network neuroscience," *Nature neuroscience*, vol. 20, no. 3, pp. 353–364, 2017.

[56] J. C. Pang *et al.*, "Geometric constraints on human brain function," *Nature*, vol. 618, no. 7965, pp. 566–574, 2023.

[57] S. Coombes *et al.*, "Modeling electrocortical activity through improved local approximations of integral neural field equations," *Physical Review E—Statistical, Nonlinear, and Soft Matter Physics*, vol. 76, no. 5, p. 051901, 2007.

[58] X.-J. Wang and H. Kennedy, "Brain structure and dynamics across scales: in search of rules," *Current opinion in neurobiology*, vol. 37, pp. 92–98, 2016.

[59] J. A. Roberts *et al.*, "Consistency-based thresholding of the human connectome," *NeuroImage*, vol. 145, pp. 118–129, 2017.

[60] S. Oldham *et al.*, "Modeling spatial, developmental, physiological, and topological constraints on human brain connectivity," *Science advances*, vol. 8, no. 22, p. eabm6127, 2022.

[61] S. Petkoski and V. K. Jirsa, "Transmission time delays organize the brain network synchronization," *Philosophical Transactions of the Royal Society A: Mathematical, Physical and Engineering Sciences*, vol. 377, no. 2153, p. 20180132, 2019.

[62] S. Petkoski and V. K. Jirsa, "Normalizing the brain connectome for communication through synchronization," *Network Neuroscience*, vol. 6, no. 3, pp. 722–744, 2022.

[63] H. Haken, "Synergetics of brain function," *International journal of psychophysiology*, vol. 60, no. 2, pp. 110–124, 2006.

[64] R. Chaudhuri *et al.*, "The intrinsic attractor manifold and population dynamics of a canonical cognitive circuit across waking and sleep," *Nature neuroscience*, vol. 22, no. 9, pp. 1512–1520, 2019.

[65] J. A. Gallego *et al.*, "Long-term stability of cortical population dynamics underlying consistent behavior," *Nature neuroscience*, vol. 23, no. 2, pp. 260–270, 2020.

[66] S. Bernardi *et al.*, "The geometry of abstraction in the hippocampus and prefrontal cortex," *Cell*, vol. 183, no. 4, pp. 954–967, 2020.

[67] E. H. Nieh *et al.*, "Geometry of abstract learned knowledge in the hippocampus," *Nature*, vol. 595, no. 7865, pp. 80–84, 2021.

[68] R. J. Gardner *et al.*, "Toroidal topology of population activity in grid cells," *Nature*, vol. 602, no. 7895, pp. 123–128, 2022.

[69] B. Sorscher *et al.*, "A unified theory for the computational and mechanistic origins of grid cells," *Neuron*, vol. 111, no. 1, pp. 121–137, 2023.

[70] C. Langdon *et al.*, "A unifying perspective on neural manifolds and circuits for cognition," *Nature Reviews Neuroscience*, vol. 24, no. 6, pp. 363–377, 2023.

[71] R. Huys *et al.*, "Functional architectures and structured flows on manifolds: a dynamical framework for motor behavior.," *Psychological review*, vol. 121, no. 3, p. 302, 2014.

[72] V. Jirsa, "Structured flows on manifolds as guiding concepts in brain science," *Selbstorganisation–ein Paradigma für die Humanwissenschaften: Zu Ehren von Günter Schiepek und seiner Forschung zu Komplexität und Dynamik in der Psychologie*, pp. 89–102, 2020.

[73] A. R. McIntosh and V. K. Jirsa, "The hidden repertoire of brain dynamics and dysfunction," *Network Neuroscience*, vol. 3, no. 4, pp. 994–1008, 2019.

[74] B. H. Jansen and V. G. Rit, "Electroencephalogram and visual evoked potential generation in a mathematical model of coupled cortical columns," *Biological cybernetics*, vol. 73, no. 4, pp. 357–366, 1995.

[75] K.-F. Wong and X.-J. Wang, "A recurrent network mechanism of time integration in perceptual decisions," *Journal of Neuroscience*, vol. 26, no. 4, pp. 1314–1328, 2006.

[76] R. A. Stefanescu and V. K. Jirsa, "A low dimensional description of globally coupled heterogeneous neural networks of excitatory and inhibitory neurons," *PLoS computational biology*, vol. 4, no. 11, p. e1000219, 2008.

[77] J. L. Hindmarsh and R. Rose, "A model of neuronal bursting using three coupled first order differential equations," *Proceedings of the Royal society of London. Series B. Biological sciences*, vol. 221, no. 1222, pp. 87–102, 1984.

[78] S. El Boustani and A. Destexhe, "A master equation formalism for macroscopic modeling of asynchronous irregular activity states," *Neural Computation*, vol. 21, p. 46–100, Jan. 2009.

[79] Y. Zerlaut *et al.*, "Heterogeneous firing rate response of mouse layer v pyramidal neurons in the fluctuation-driven regime," *The Journal of Physiology*, vol. 594, p. 3791–3808, June 2016.

[80] M. Carlu *et al.*, "A mean-field approach to the dynamics of networks of complex neurons, from nonlinear integrate-and-fire to hodgkin–huxley models," *Journal of Neurophysiology*, vol. 123, pp. 1042–1051, Mar. 2020.

[81] C. G. Alexandersen *et al.*, "A mean field to capture asynchronous irregular dynamics of conductance-based networks of adaptive quadratic integrate-and-fire neuron models," *Neural Computation*, vol. 36, pp. 1433–1448, June 2024.

[82] V. K. Jirsa *et al.*, "On the nature of seizure dynamics.," *Brain : a journal of neurology*, vol. 137, pp. 2210–30, 8 2014.

[83] E. Montbrió *et al.*, "Macroscopic description for networks of spiking neurons," *Physical Review X*, vol. 5, June 2015.

[84] D. Depannemaecker *et al.*, "A neural mass model with neuromodulation," *bioRxiv*, pp. 2024–06, 2024.

[85] L. Chen and S. A. Campbell, "Exact mean-field models for spiking neural networks with adaptation," *Journal of Computational Neuroscience*, vol. 50, p. 445–469, July 2022.

[86] P. Sanz-Leon *et al.*, "Mathematical framework for large-scale brain network modeling in the virtual brain," *Neuroimage*, vol. 111, pp. 385–430, 2015.

[87] R. FitzHugh, "Impulses and physiological states in theoretical models of nerve membrane," *Biophysical journal*, vol. 1, no. 6, pp. 445–466, 1961.

[88] J. Nagumo, S. Arimoto, and S. Yoshizawa, "An active pulse transmission line simulating nerve axon," *Proceedings of the IRE*, vol. 50, no. 10, pp. 2061–2070, 1962.

[89] C. Morris and H. Lecar, "Voltage oscillations in the barnacle giant muscle fiber," *Biophysical journal*, vol. 35, no. 1, pp. 193–213, 1981.

[90] G. Deco *et al.*, "The dynamic brain: from spiking neurons to neural masses and cortical fields," *PLoS computational biology*, vol. 4, no. 8, p. e1000092, 2008.

[91] K. L. Miller *et al.*, "High-resolution fmri at 1.5 t using balanced ssfp," *Magnetic Resonance in Medicine: An Official Journal of the International Society for Magnetic Resonance in Medicine*, vol. 55, no. 1, pp. 161–170, 2006.

[92] F. De Martino *et al.*, "Whole brain high-resolution functional imaging at ultra high magnetic fields: an application to the analysis of resting state networks," *Neuroimage*, vol. 57, no. 3, pp. 1031–1044, 2011.

[93] I. Levy *et al.*, "One picture is worth at least a million neurons," *Current Biology*, vol. 14, no. 11, pp. 996–1001, 2004.

[94] G. M. Edelman and J. A. Gally, "Degeneracy and complexity in biological systems," *Proceedings of the National Academy of Sciences*, vol. 98, pp. 13763–13768, 11 2001.

[95] M. Betancourt, "A conceptual introduction to hamiltonian monte carlo," *arXiv*, 2017.

[96] M. Breakspear, "Dynamic models of large-scale brain activity," *Nature neuroscience*, vol. 20, no. 3, pp. 340–352, 2017.

[97] M. Ramezanian-Panahi *et al.*, "Generative models of brain dynamics," *Frontiers in artificial intelligence*, vol. 5, p. 807406, 2022.

[98] D. Depannemaecker *et al.*, "From phenomenological to biophysical models of seizures," *Neurobiology of Disease*, vol. 182, p. 106131, June 2023.

[99] G. Rabuffo *et al.*, "Biophysically inspired mean-field model of neuronal populations driven by ion exchange mechanisms," *eLife*, vol. 14, 2025.

[100] M. L. Saggio and V. K. Jirsa, "Phenomenological mesoscopic for seizure activity models," *A Complex Systems Approach to Epilepsy: Concept, Practice, and Therapy*, p. 41, 2023.

[101] D. T. Liley *et al.*, "A spatially continuous mean fieldtheory of electrocortical activity," *Network: Computation in Neural Systems*, vol. 13, no. 1, p. 67, 2001.

[102] Á. Byrne *et al.*, "Next-generation neural mass and field modeling," *Journal of neurophysiology*, vol. 123, no. 2, pp. 726–742, 2020.

[103] S. Coombes, "Next generation neural population models," *Frontiers in Applied Mathematics and Statistics*, vol. 9, p. 1128224, 2023.

[104] R. Gast *et al.*, "Macroscopic dynamics of neural networks with heterogeneous spiking thresholds," *Physical Review E*, vol. 107, Feb. 2023.

[105] R. Curtu and B. Ermentrout, "Pattern formation in a network of excitatory and inhibitory cells with adaptation," *SIAM Journal on Applied Dynamical Systems*, vol. 3, no. 3, pp. 191–231, 2004.

[106] N. Brunel and X.-J. Wang, "Effects of neuromodulation in a cortical network model of object working memory dominated by recurrent inhibition," *Journal of computational neuroscience*, vol. 11, pp. 63–85, 2001.

[107] M. Hashemi *et al.*, "Anesthetic action on extra-synaptic receptors: effects in neural population models of eeg activity," *Frontiers in Systems Neuroscience*, vol. 8, p. 232, 2014.

[108] M. L. Saggio *et al.*, "Fast–Slow Bursters in the Unfolding of a High Codimension Singularity and the Ultra-slow Transitions of Classes," *The Journal of Mathematical Neuroscience*, vol. 7, no. 1, p. 7, 2017.

[109] S. N. Kalitzin *et al.*, "Stimulation-based anticipation and control of state transitions in the epileptic brain," *Epilepsy & Behavior*, vol. 17, no. 3, pp. 310–323, 2010.

[110] L. Kusch *et al.*, "Dynamics and bifurcation structure of a mean-field model of adaptive exponential integrate-and-fire networks," *BioArXiv*, Dec. 2023.

[111] E. C. A. Hansen *et al.*, "Functional connectivity dynamics: modeling the switching behavior of the resting state," *Neuroimage*, vol. 105, pp. 525–535, Jan. 2015.

[112] G. Rabuffo *et al.*, "Neuronal Cascades Shape Whole-Brain Functional Dynamics at Rest," *eNeuro*, vol. 8, Sept. 2021.

[113] J. Tabak *et al.*, "Modeling of spontaneous activity in developing spinal cord using activity-dependent depression in an excitatory network," *Journal of Neuroscience*, vol. 20, no. 8, pp. 3041–3056, 2000.

[114] N. Brunel and X.-J. Wang, "Effects of neuromodulation in a cortical network model of object working memory dominated by recurrent inhibition," *Journal of computational neuroscience*, vol. 11, pp. 63–85, 2001.

[115] J. Courtiol *et al.*, "Dynamical mechanisms of interictal resting-state functional connectivity in epilepsy," *Journal of Neuroscience*, vol. 40, no. 29, pp. 5572–5588, 2020.

[116] F. Wendling *et al.*, "Computational models of epileptiform activity," *Journal of neuroscience methods*, vol. 260, pp. 233–251, 2016.

[117] P. N. Taylor *et al.*, "Structural connectivity based whole brain modelling in epilepsy," *Journal of neuroscience methods*, vol. 236, pp. 51–57, 2014.

[118] F. Hutchings *et al.*, "Predicting surgery targets in temporal lobe epilepsy through structural connectome based simulations," *PLoS computational biology*, vol. 11, no. 12, p. e1004642, 2015.

[119] M. Goodfellow *et al.*, "Estimation of brain network ictogenicity predicts outcome from epilepsy surgery," *Scientific reports*, vol. 6, no. 1, p. 29215, 2016.

[120] N. Sinha *et al.*, "Predicting neurosurgical outcomes in focal epilepsy patients using computational modelling," *Brain*, vol. 140, no. 2, pp. 319–332, 2017.

[121] T. Proix *et al.*, "Individual brain structure and modelling predict seizure propagation," *Brain*, vol. 140, no. 3, pp. 641–654, 2017.

[122] T. Proix *et al.*, "Predicting the spatiotemporal diversity of seizure propagation and termination in human focal epilepsy," *Nature communications*, vol. 9, no. 1, p. 1088, 2018.

[123] M. Gerster *et al.*, "Patient-specific network connectivity combined with a next generation neural mass model to test clinical hypothesis of seizure propagation," *Frontiers in Systems Neuroscience*, vol. 15, p. 675272, 2021.

[124] F. H. L. da Silva *et al.*, "Dynamical diseases of brain systems: different routes to epileptic seizures," *IEEE transactions on biomedical engineering*, vol. 50, no. 5, pp. 540–548, 2003.

[125] G. Baier *et al.*, "The importance of modeling epileptic seizure dynamics as spatio-temporal patterns," *Frontiers in physiology*, vol. 3, p. 281, 2012.

[126] S. Kalitzin *et al.*, "Computational model prospective on the observation of proictal states in epileptic neuronal systems," *Epilepsy & Behavior*, vol. 22, pp. S102–S109, 2011.

[127] E. M. Izhikevich, "Neural excitability, spiking and bursting," *International journal of bifurcation and chaos*, vol. 10, no. 06, pp. 1171–1266, 2000.

[128] M. L. Saggio *et al.*, "A taxonomy of seizure dynamotypes," *eLife*, vol. 9, July 2020.

[129] K. El Houssaini *et al.*, "The epileptor model: a systematic mathematical analysis linked to the dynamics of seizures, refractory status epilepticus, and depolarization block," *Eneuro*, vol. 7, no. 2, 2020.

[130] M. L. Saggio and V. Jirsa, "Bifurcations and bursting in the epileptor," *PLOS Computational Biology*, vol. 20, no. 3, p. e1011903, 2024.

[131] F. Wendling *et al.*, "Epileptic fast activity can be explained by a model of impaired gabaergic dendritic inhibition," *European Journal of Neuroscience*, vol. 15, no. 9, pp. 1499–1508, 2002.

[132] T. L. Eissa *et al.*, "Cross-scale effects of neural interactions during human neocortical seizure activity," *Proceedings of the National Academy of Sciences*, vol. 114, no. 40, pp. 10761–10766, 2017.

[133] K. E. Houssaini *et al.*, "Seizures, refractory status epilepticus, and depolarization block as endogenous brain activities," *Physical Review E*, vol. 91, pp. 2–6, 2015.

[134] M. Golubitsky *et al.*, "An unfolding theory approach to bursting in fast–slow systems," in *Global analysis of dynamical systems*, pp. 282–313, CRC Press, 2001.

[135] H. M. Osinga *et al.*, "Cross-currents between biology and mathematics: The codimension of pseudo-plateau bursting," vol. 32, no. 8, p. 2853, 2012.

[136] S. L. Brunton and J. N. Kutz, "7 Data-driven methods for reduced-order modeling," in *Volume 2 Snapshot-Based Methods and Algorithms: Volume 2: Snapshot-Based Methods and Algorithms* (P. Benner, S. Grivet-Talocia, A. Quarteroni, G. Rozza, W. Schilders, and L. M. Silveira, eds.), pp. 307–344, De Gruyter, Dec. 2020.

[137] M. Verhaegen and V. Verdult, *Filtering and System Identification: A Least Squares Approach*. Cambridge: Cambridge University Press, first paperback edition ed., 2011.

[138] E. Nozari *et al.*, "Macroscopic resting-state brain dynamics are best described by linear models," *Nat. Biomed. Eng*, vol. 8, pp. 68–84, Jan. 2024.

[139] D. Durstewitz *et al.*, "Reconstructing computational system dynamics from neural data with recurrent neural networks," *Nat. Rev. Neurosci.*, vol. 24, pp. 693–710, Nov. 2023.

[140] S. Hochreiter and J. Schmidhuber, "Long Short-Term Memory," *Neural Comput.*, vol. 9, pp. 1735–1780, Nov. 1997.

[141] K. Cho *et al.*, "Learning Phrase Representations using RNN Encoder-Decoder for Statistical Machine Translation," Sept. 2014.

[142] R. T. Q. Chen *et al.*, "Neural Ordinary Differential Equations," in *Advances in Neural Information Processing Systems*, vol. 31, Curran Associates, Inc., 2018.

[143] S. L. Brunton *et al.*, "Discovering governing equations from data by sparse identification of nonlinear dynamical systems," *Proc. Natl. Acad. Sci. U.S.A.*, vol. 113, pp. 3932–3937, Apr. 2016.

[144] V. Sip *et al.*, "Data-driven method to infer the seizure propagation patterns in an epileptic brain from intracranial electroencephalography," *PLOS Computational Biology*, vol. 17, p. e1008689, 2 2021.

[145] N. Baldy *et al.*, "Inference on the macroscopic dynamics of spiking neurons," *Neural Computation*, pp. 1–43, 08 2024.

[146] V. Sip *et al.*, "Characterization of regional differences in resting-state fMRI with a data-driven network model of brain dynamics," *Science Advances*, vol. 9, p. eabq7547, Mar. 2023.

[147] F. Melozzi *et al.*, "Individual structural features constrain the mouse functional connectome," *Proceedings of the National Academy of Sciences*, vol. 116, no. 52, pp. 26961–26969, 2019.

[148] M. Schirner *et al.*, "An automated pipeline for constructing personalized virtual brains from multimodal neuroimaging data," *NeuroImage*, vol. 117, pp. 343 – 357, 2015.

[149] F. Zhang *et al.*, "Quantitative mapping of the brain's structural connectivity using diffusion MRI tractography: A review," *NeuroImage*, vol. 249, p. 118870, Apr. 2022.

[150] M. Hashemi *et al.*, "Anesthetic action on the transmission delay between cortex and thalamus explains the beta-buzz observed under propofol anesthesia," *PLoS One*, vol. 12, no. 6, p. e0179286, 2017.

[151] S. Petkoski *et al.*, "Phase-lags in large scale brain synchronization: Methodological considerations and in-silico analysis," *PLoS Computational Biology*, vol. 14, no. 7, pp. 1–30, 2018.

[152] V. Jirsa, "Connectivity and dynamics of neural information processing," *Neuroinformatics*, vol. 2, no. 2, pp. 183–204, 2004.

[153] D. Daini *et al.*, "Spherical-harmonics mode decomposition of neural field equations," *Physical Review E*, vol. 101, no. 1, p. 12202, 2020. Publisher: American Physical Society.

[154] A. N. Vattikonda *et al.*, "Improving epileptogenic zone estimation using bayesian inference on neural field models," *medRxiv*, pp. 2023–10, 2023.

[155] L. Muller *et al.*, "Cortical travelling waves: mechanisms and computational principles," *Nature Reviews Neuroscience*, vol. 19, pp. 255–268, May 2018.

[156] S. An *et al.*, "High-resolution virtual brain modeling personalizes deep brain stimulation for treatment-resistant depression: Spatiotemporal response characteristics following stimulation of neural fiber pathways," *Neuroimage*, vol. 249, p. 118848, 2022.

[157] E. M. Hillman, "Coupling Mechanism and Significance of the BOLD Signal: A Status Report," *Annual Review of Neuroscience*, vol. 37, pp. 161–181, July 2014.

[158] P. J. Drew, "Vascular and neural basis of the BOLD signal," *Current Opinion in Neurobiology*, vol. 58, pp. 61–69, Oct. 2019.

[159] K. Friston *et al.*, "Nonlinear Responses in fMRI: The Balloon Model, Volterra Kernels, and Other Hemodynamics," *NeuroImage*, vol. 12, pp. 466–477, Oct. 2000. Publisher: Elsevier BV.

[160] R. B. Buxton, "Dynamic models of BOLD contrast," *NeuroImage*, vol. 62, pp. 953–961, Aug. 2012.

[161] J. H. Kim and D. Ress, "Arterial impulse model for the BOLD response to brief neural activation," *NeuroImage*, vol. 124, pp. 394–408, Jan. 2016.

[162] J. R. Polimeni and L. D. Lewis, "Imaging faster neural dynamics with fast fMRI: A need for updated models of the hemodynamic response," *Progress in Neurobiology*, vol. 207, p. 102174, Dec. 2021.

[163] D. A. Handwerker *et al.*, "Variation of BOLD hemodynamic responses across subjects and brain regions and their effects on statistical analyses," *NeuroImage*, vol. 21, pp. 1639–1651, Apr. 2004.

[164] A. J. Taylor *et al.*, "Characterization of the hemodynamic response function across the majority of human cerebral cortex," *NeuroImage*, vol. 173, pp. 322–331, June 2018.

[165] W. M. Zhu *et al.*, "Neurovascular coupling mechanisms in health and neurovascular uncoupling in Alzheimer's disease," *Brain*, vol. 145, pp. 2276–2292, July 2022.

[166] K. L. West *et al.*, "BOLD hemodynamic response function changes significantly with healthy aging," *NeuroImage*, vol. 188, pp. 198–207, Mar. 2019.

[167] G. Buzsáki *et al.*, "The origin of extracellular fields and currents-EEG, ECoG, LFP and spikes," *Nature Reviews Neuroscience*, vol. 13, no. 6, pp. 407–420, 2012. arXiv: NIHMS150003 Publisher: Nature Publishing Group ISBN: 1471-0048 (Electronic)\r1471-003X (Linking).

[168] J. Sarvas, "Basic mathematical and electromagnetic concepts of the biomagnetic inverse problem," *Physics in Medicine & Biology*, vol. 32, no. 1, p. 11, 1987.

[169] H. Hallez *et al.*, "Review on solving the forward problem in EEG source analysis," *Journal of NeuroEngineering and Rehabilitation*, vol. 4, 2007.

[170] R. Henson *et al.*, "Selecting forward models for MEG source-reconstruction using model-evidence," *NeuroImage*, vol. 46, pp. 168–176, May 2009.

[171] C. H. Wolters *et al.*, "Influence of tissue conductivity anisotropy on EEG/MEG field and return current computation in a realistic head model: A simulation and visualization study using high-resolution finite element modeling," *NeuroImage*, vol. 30, no. 3, pp. 813–826, 2006.

[172] S. Næss *et al.*, "Biophysically detailed forward modeling of the neural origin of EEG and MEG signals," *NeuroImage*, vol. 225, p. 117467, Jan. 2021. Publisher: Elsevier BV.

[173] A. Gramfort, "MEG and EEG data analysis with MNE-Python," *Frontiers in Neuroscience*, vol. 7, 2013.

[174] F. Tadel *et al.*, "Brainstorm : A User-Friendly Application for MEG / EEG Analysis," *Computational Intelligence and Neuroscience*, vol. 2011, 2011.

[175] R. Oostenveld *et al.*, "FieldTrip: Open Source Software for Advanced Analysis of MEG, EEG, and Invasive Electrophysiological Data," *Computational Intelligence and Neuroscience*, vol. 2011, pp. 1–9, 2011. Publisher: Wiley.

[176] A. Gramfort *et al.*, "Forward field computation with OpenMEEG," *Computational Intelligence and Neuroscience*, vol. 2011, no. June 2014, 2011. ISBN: 1687-5273 (Electronic).

[177] C. M. Tax *et al.*, "What's new and what's next in diffusion MRI preprocessing," *NeuroImage*, vol. 249, p. 118830, Apr. 2022.

[178] D. A. Dickie *et al.*, "Whole Brain Magnetic Resonance Image Atlases: A Systematic Review of Existing Atlases and Caveats for Use in Population Imaging," *Frontiers in Neuroinformatics*, vol. 11, Jan. 2017.

[179] S. N. Sotiropoulos and A. Zalesky, "Building connectomes using diffusion MRI: why, how and but," *NMR in Biomedicine*, vol. 32, p. e3752, Apr. 2017.

[180] S. Medina Villalon *et al.*, "EpiTools, A software suite for presurgical brain mapping in epilepsy: Intracerebral EEG," *Journal of Neuroscience Methods*, vol. 303, pp. 7–15, 2018. Publisher: Elsevier B.V.

[181] R. Butler *et al.*, "Application of polymer sensitive MRI sequence to localization of EEG electrodes," *Journal of Neuroscience Methods*, vol. 278, pp. 36–45, Feb. 2017.

[182] D. Kristanto *et al.*, "The multiverse of data preprocessing and analysis in graph-based fMRI: A systematic literature review of analytical choices fed into a decision support tool for informed analysis," *Neuroscience & Biobehavioral Reviews*, vol. 165, p. 105846, Oct. 2024.

[183] A. I. Luppi *et al.*, "Systematic evaluation of fMRI data-processing pipelines for consistent functional connectomics," *Nature Communications*, vol. 15, p. 4745, June 2024.

[184] A. Puce and M. Hämäläinen, "A Review of Issues Related to Data Acquisition and Analysis in EEG/MEG Studies," *Brain Sciences*, vol. 7, p. 58, May 2017.

[185] A. Sorrentino and M. Piana, "Inverse Modeling for MEG/EEG Data," in *Mathematical and Theoretical Neuroscience* (G. Naldi and T. Nieus, eds.), vol. 24, pp. 239–253, Cham: Springer International Publishing, 2017. Series Title: Springer INdAM Series.

[186] R. Botvinik-Nezer *et al.*, "Variability in the analysis of a single neuroimaging dataset by many teams," *Nature*, vol. 582, pp. 84–88, June 2020.

[187] C. Maffei *et al.*, "Insights from the irontract challenge: Optimal methods for mapping brain pathways from multi-shell diffusion mri," *NeuroImage*, vol. 257, p. 119327, 2022.

[188] K. H. Maier-Hein *et al.*, "The challenge of mapping the human connectome based on diffusion tractography," *Nature Communications*, vol. 8, no. 1, 2017.

[189] D. Trübutschek *et al.*, "EEGManyPipelines: A Large-scale, Grassroots Multi-analyst Study of Electroencephalography Analysis Practices in the Wild," *Journal of Cognitive Neuroscience*, vol. 36, pp. 217–224, Feb. 2024.

[190] R. R. Cruces *et al.*, "Micapipe: A pipeline for multimodal neuroimaging and connectome analysis," *NeuroImage*, vol. 263, p. 119612, Nov. 2022.

[191] O. Esteban *et al.*, "fMRIPrep: a robust preprocessing pipeline for functional MRI," *Nature Methods*, vol. 16, no. 1, pp. 111–116, 2019. Publisher: Springer US.

[192] K. Mehta *et al.*, "XCP-D: A Robust Pipeline for the post-processing of fMRI data," Nov. 2023.

[193] R. Smith and A. Conelly, "MRtrix3_connectome: A BIDS Application for quantitative structural connectome constructi," vol. 610, 2019.

[194] M. F. Glasser *et al.*, "The minimal preprocessing pipelines for the Human Connectome Project," *NeuroImage*, vol. 80, pp. 105–124, 2013. Publisher: Elsevier Inc.

[195] N. Frazier-Logue *et al.*, "A Robust Modular Automated Neuroimaging Pipeline for Model Inputs to TheVirtualBrain," *Frontiers in Neuroinformatics*, vol. 16, p. 883223, June 2022.

[196] P. Sanz Leon *et al.*, "The virtual brain: a simulator of primate brain network dynamics," *Frontiers in neuroinformatics*, vol. 7, p. 10, 2013.

[197] M. Schirner *et al.*, "Brain simulation as a cloud service: The virtual brain on ebrains," *NeuroImage*, vol. 251, p. 118973, 2022.

[198] M. Schirner *et al.*, "Inferring multi-scale neural mechanisms with brain network modelling," *eLife*, vol. 7, p. e28927, 8 Jan. 2018.

[199] I. Martín *et al.*, "TVB C++: A fast and flexible Back-End for The Virtual Brain," *arXiv [q-bio.NC]*, 29 May 2024.

[200] van der Vlag *et al.*, "RateML: A code generation tool for brain network models," *Front. Netw. Physiol.*, vol. 2, p. 826345, 14 Feb. 2022.

[201] J. Fousek, "Efficient sparse matrix-delayed vector multiplication for discretized neural field model," *J. Supercomput.*, vol. 74, pp. 1863–1884, 1 May 2018.

[202] E. D'Angelo and V. Jirsa, "The quest for multiscale brain modeling," *Trends in neurosciences*, 2022.

[203] A. Gelman *et al.*, *Bayesian data analysis*. CRC press, 2013.

[204] C. M. Bishop, *Pattern Recognition and Machine Learning*. Springer, 2006.

[205] K. J. Friston *et al.*, "Computational psychiatry: the brain as a phantastic organ," *The Lancet Psychiatry*, vol. 1, pp. 148–158, 2014.

[206] J. Pearl, "Causal inference in statistics: An overview," *Statistics Surveys*, vol. 3, no. none, pp. 96 – 146, 2009.

[207] A. Esmaeili *et al.*, "Probing other's presence: Probabilistic inference across brain scales reveals enhanced excitatory synaptic efficacy," *bioRxiv*, pp. 2024–09, 2024.

[208] M. Hashemi *et al.*, "On the influence of prior information evaluated by fully bayesian criteria in a personalized whole-brain model of epilepsy spread," *PLoS computational biology*, vol. 17, no. 7, p. e1009129, 2021.

[209] N. Baldy *et al.*, "Hierarchical bayesian pharmacometrics analysis of baclofen for alcohol use disorder," *Machine Learning: Science and Technology*, 2023.

[210] R. van de Schoot *et al.*, "Bayesian statistics and modelling," *Nature Reviews Methods Primers*, vol. 1, no. 1, p. 1, 2021.

[211] A. Gelman *et al.*, "Understanding predictive information criteria for bayesian models," *Stat. Comput.*, vol. 24, pp. 997–1016, Nov. 2014.

[212] A. Vehtari *et al.*, "Practical bayesian model evaluation using leave-one-out cross-validation and WAIC," *Stat. Comput.*, vol. 27, pp. 1413–1432, Sept. 2017.

[213] K. J. Friston *et al.*, "Dynamic causal modelling," *Neuroimage*, vol. 19, no. 4, pp. 1273–1302, 2003.

[214] K. J. Friston, "The free-energy principle: a unified brain theory?," *Nature reviews neuroscience*, vol. 11, no. 2, pp. 127–138, 2010.

[215] O. David *et al.*, "Dynamic causal modeling of evoked responses in eeg and meg," *NeuroImage*, vol. 30, no. 4, pp. 1255–1272, 2006.

[216] K. J. Friston *et al.*, "Variational free energy and the laplace approximation," *Neuroimage*, vol. 34, no. 1, pp. 220–234, 2007.

[217] P. Zeidman *et al.*, "A primer on Variational Laplace (VL)," *NeuroImage*, vol. 279, p. 120310, 2023.

[218] M. Hashemi *et al.*, "The bayesian virtual epileptic patient: A probabilistic framework designed to infer the spatial map of epileptogenicity in a personalized large-scale brain model of epilepsy spread," *NeuroImage*, vol. 217, p. 116839, 8 2020.

[219] M. Hashemi *et al.*, "Amortized bayesian inference on generative dynamical network models of epilepsy using deep neural density estimators," *Neural Networks*, vol. 163, pp. 178–194, 6 2023.

[220] M. Hashemi *et al.*, "Simulation-based inference on virtual brain models of disorders," *Machine Learning: Science and Technology*, vol. 5, p. 035019, jul 2024.

[221] S. Brooks *et al.*, *Handbook of Markov Chain Monte Carlo. Handbooks of Modern Statistical Methods*. London, UK: Hall/CRC, 2011.

[222] M. Hashemi *et al.*, "Optimal model parameter estimation from eeg power spectrum features observed during general anesthesia," *Neuroinformatics*, vol. 16, pp. 231–251, 2018.

[223] A. N. Vattikonda *et al.*, "Identifying spatio-temporal seizure propagation patterns in epilepsy using bayesian inference," *Communications Biology*, vol. 4, p. 1244, 12 2021.

[224] M. D. Hoffman and A. Gelman, "The no-u-turn sampler: Adaptively setting path lengths in hamiltonian monte carlo," *J. Mach. Learn. Res.*, vol. 15, pp. 1593–1623, Jan. 2014.

[225] B. Carpenter *et al.*, "Stan: A probabilistic programming language," *Journal of Statistical Software, Articles*, vol. 76, no. 1, pp. 1–32, 2017.

[226] J. Jha *et al.*, "Fully bayesian estimation of virtual brain parameters with self-tuning hamiltonian monte carlo," *Machine Learning: Science and Technology*, vol. 3, p. 035016, 9 2022.

[227] D. R. Penas *et al.*, "Parameter estimation in a whole-brain network model of epilepsy: Comparison of parallel global optimization solvers," *PLOS Computational Biology*, vol. 20, no. 7, p. e1011642, 2024.

[228] J.-D. Lemaréchal *et al.*, "Effects of the spatial resolution of the virtual epileptic patient on the identification of epileptogenic networks," *Imaging Neuroscience*, vol. 2, pp. 1–22, 2024.

[229] K. Cranmer *et al.*, "The frontier of simulation-based inference," *Proceedings of the National Academy of Sciences*, vol. 117, pp. 30055–30062, 12 2020.

[230] P. J. Gonçalves *et al.*, "Training deep neural density estimators to identify mechanistic models of neural dynamics," *Elife*, vol. 9, p. e56261, 2020.

[231] G. Papamakarios *et al.*, "Masked autoregressive flow for density estimation," *Advances in neural information processing systems*, vol. 30, 2017.

[232] C. Durkan *et al.*, "Neural spline flows," *Advances in Neural Information Processing Systems*, vol. 32, pp. 7511–7522, 2019.

[233] B. H. Yalcinkaya *et al.*, "Personalized virtual brains of alzheimer's disease link dynamical biomarkers of fmri with increased local excitability," *medRxiv*, pp. 2023–01, 2023.

[234] G. Rabuffo *et al.*, "Probing the mechanisms of global brain reconfiguration after local manipulations," *bioRxiv*, pp. 2023–09, 2023.

[235] K. J. Friston *et al.*, "Statistical parametric maps in functional imaging: a general linear approach," *Human Brain Mapping*, vol. 2, no. 4, pp. 189–210, 1994.

[236] W. D. Penny, "Comparing dynamic causal models using AIC, BIC and free energy," *Neuroimage*, vol. 59, pp. 319–330, Jan. 2012.

[237] D. A. Gusnard *et al.*, "Searching for a baseline: functional imaging and the resting human brain," *Nat. Rev. Neurosci.*, vol. 2, pp. 685–694, Oct. 2001.

[238] J. S. Damoiseaux *et al.*, "Consistent resting-state networks across healthy subjects," *Proc. Natl. Acad. Sci. U. S. A.*, vol. 103, pp. 13848–13853, Sept. 2006.

[239] R. M. Hutchison *et al.*, "Dynamic functional connectivity: promise, issues, and interpretations," *Neuroimage*, vol. 80, pp. 360–378, 2013.

[240] M. G. Preti *et al.*, "The dynamic functional connectome: State-of-the-art and perspectives," *Neuroimage*, vol. 160, pp. 41–54, Oct. 2017.

[241] J. M. Shine *et al.*, "The Dynamics of Functional Brain Networks: Integrated Network States during Cognitive Task Performance," *Neuron*, vol. 92, pp. 544–554, Oct. 2016.

[242] D. T. Jones *et al.*, "Non-stationarity in the "resting brain's" modular architecture," *PLoS One*, vol. 7, p. e39731, June 2012.

[243] L. Arbabyazd *et al.*, "State-switching and high-order spatiotemporal organization of dynamic functional connectivity are disrupted by Alzheimer's disease," *Network Neuroscience*, pp. 1–32, 2023.

[244] D. Dong *et al.*, "Dysfunction of large-scale brain networks in schizophrenia: A meta-analysis of resting-state functional connectivity," *Schizophr. Bull.*, vol. 44, pp. 168–181, 13 Jan. 2018.

[245] A. T. Drysdale *et al.*, "Resting-state connectivity biomarkers define neurophysiological subtypes of depression," *Nat. Med.*, vol. 23, pp. 28–38, Jan. 2017.

[246] D. Battaglia *et al.*, "Dynamic Functional Connectivity between order and randomness and its evolution across the human adult lifespan," *Neuroimage*, vol. 222, p. 117156, Nov. 2020.

[247] S. Petkoski *et al.*, "White-matter degradation and dynamical compensation support age-related functional alterations in human brain," *Cerebral Cortex*, vol. bhac500, pp. 1–16, 2023.

[248] F. Cavanna *et al.*, "Dynamic functional connectivity and brain metastability during altered states of consciousness," *Neuroimage*, vol. 180, pp. 383–395, Oct. 2018.

[249] A. Demertzi *et al.*, "Human consciousness is supported by dynamic complex patterns of brain signal coordination," *Science Advances*, vol. 5, no. 2, pp. 1–12, 2019.

[250] J. M. Shine, "Neuromodulatory Influences on Integration and Segregation in the Brain," *Trends in Cognitive Sciences*, vol. 23, no. 7, pp. 572–583, 2019.

[251] C. J. Stam *et al.*, "Network hyperexcitability in early Alzheimer's disease: Is functional connectivity a potential biomarker?," *Brain Topogr.*, vol. 36, pp. 595–612, July 2023.

[252] D. Azzalini *et al.*, "Visceral signals shape brain dynamics and cognition," *Trends in cognitive sciences*, vol. 23, no. 6, pp. 488–509, 2019.

[253] M. Thiebaut de Schotten and S. J. Forkel, "The emergent properties of the connected brain," *Science*, vol. 378, no. 6619, pp. 505–510, 2022.

[254] J. O'Byrne and K. Jerbi, "How critical is brain criticality?," *Trends in Neurosciences*, vol. 45, no. 11, pp. 820–837, 2022.

[255] L. Cocchi *et al.*, "Criticality in the brain: A synthesis of neurobiology, models and cognition," *Prog. Neurobiol.*, vol. 158, pp. 132–152, Nov. 2017.

[256] F. Z. Esfahlani *et al.*, "High-amplitude cofluctuations in cortical activity drive functional connectivity," *Proc. Natl. Acad. Sci. U. S. A.*, vol. 117, pp. 28393–28401, Nov. 2020.

[257] M. Pope *et al.*, "Modular origins of high-amplitude cofluctuations in fine-scale functional connectivity dynamics," *Proceedings of the National Academy of Sciences*, vol. 118, no. 46, p. e2109380118, 2021.

[258] M. Breyton *et al.*, "Spatiotemporal brain complexity quantifies consciousness outside of perturbation paradigms," Aug. 2024.

[259] Gutierrez-Barragan *et al.*, "Evolutionarily conserved fmri network dynamics in the mouse, macaque, and human brain," *bioRxiv*, pp. 2023–07, 2023.

[260] T. Watanabe *et al.*, "A pairwise maximum entropy model accurately describes resting-state human brain networks," *Nature communications*, vol. 4, no. 1, pp. 1–10, 2013.

[261] S. Gu *et al.*, "The Energy Landscape of Neurophysiological Activity Implicit in Brain Network Structure," *Sci. Rep.*, vol. 8, p. 2507, Feb. 2018.

[262] P. beim Graben *et al.*, "Metastable resting state brain dynamics," *Frontiers in Computational Neuroscience*, vol. 13, 2019.

[263] E. J. Cornblath *et al.*, "Temporal sequences of brain activity at rest are constrained by white matter structure and modulated by cognitive demands," *Commun Biol*, vol. 3, p. 261, May 2020.

[264] A. Ashourvan *et al.*, "The energy landscape underpinning module dynamics in the human brain connectome," *Neuroimage*, vol. 157, pp. 364–380, 2017.

[265] J. Vohryzek *et al.*, "Ghost Attractors in Spontaneous Brain Activity: Recurrent Excursions Into Functionally-Relevant BOLD Phase-Locking States," *Front. Syst. Neurosci.*, vol. 14, p. 20, Apr. 2020.

[266] A. R. McIntosh and V. K. Jirsa, "The hidden repertoire of brain dynamics and dysfunction," *Network Neuroscience*, vol. 3, no. 4, pp. 994–1008, 2019.

[267] S. Casarotto *et al.*, "Stratification of unresponsive patients by an independently validated index of brain complexity," *Annals of neurology*, vol. 80, no. 5, pp. 718–729, 2016.

[268] C. Gratton *et al.*, "Focal brain lesions to critical locations cause widespread disruption of the modular organization of the brain," *Journal of cognitive neuroscience*, vol. 24, no. 6, pp. 1275–1285, 2012.

[269] F. Rocchi *et al.*, "Increased fmri connectivity upon chemogenetic inhibition of the mouse prefrontal cortex," *Nature communications*, vol. 13, no. 1, p. 1056, 2022.

[270] C. Elorette *et al.*, "The neural basis of resting-state fmri functional connectivity in fronto-limbic circuits revealed by chemogenetic manipulation," *Nature Communications*, vol. 15, no. 1, p. 4669, 2024.

[271] L. M. Peeters *et al.*, "Chemogenetic silencing of neurons in the mouse anterior cingulate area modulates neuronal activity and functional connectivity," *Neuroimage*, vol. 220, p. 117088, 2020.

[272] M. I. Falcon *et al.*, "The virtual brain: modeling biological correlates of recovery after chronic stroke," *Frontiers in neurology*, vol. 6, p. 228, 2015.

[273] R. A. Bethlehem *et al.*, "Brain charts for the human lifespan," *Nature*, vol. 604, no. 7906, pp. 525–533, 2022.

[274] L. Sun *et al.*, "Functional connectome through the human life span," *BioRxiv*, 2023.

[275] J. Stumme *et al.*, "Functional network reorganization in older adults: Graph-theoretical analyses of age, cognition and sex," *NeuroImage*, vol. 214, no. February, p. 116756, 2020.

[276] R. F. Betzel *et al.*, "Changes in structural and functional connectivity among resting-state networks across the human lifespan," *NeuroImage*, vol. 102, no. P2, pp. 345–357, 2014.

[277] J. Zimmermann *et al.*, "Structural architecture supports functional organization in the human aging brain at a regionwise and network level," *Human Brain Mapping*, vol. 37, no. 7, pp. 2645–2661, 2016.

[278] T. T. Nakagawa *et al.*, "Bottom up modeling of the connectome: Linking structure and function in the resting brain and their changes in aging," *NeuroImage*, vol. 80, pp. 318–329, 2013.

[279] S. Caspers *et al.*, "Studying variability in human brain aging in a population-based german cohort—rationale and design of 1000brains," *Frontiers in aging neuroscience*, vol. 6, p. 149, 2014.

[280] S. Naik *et al.*, "Metastability in senescence," *Trends in cognitive sciences*, vol. 21, no. 7, pp. 509–521, 2017.

[281] A. S. Berry *et al.*, "Aging affects dopaminergic neural mechanisms of cognitive flexibility," *Journal of Neuroscience*, vol. 36, no. 50, pp. 12559–12569, 2016.

[282] P. A. Reuter-Lorenz and D. C. Park, "How does it stac up? revisiting the scaffolding theory of aging and cognition," *Neuropsychology review*, vol. 24, pp. 355–370, 2014.

[283] H. Lassmann, "Multiple sclerosis pathology," *Cold Spring Harbor perspectives in medicine*, vol. 8, no. 3, p. a028936, 2018.

[284] D. Mollison *et al.*, "The clinico-radiological paradox of cognitive function and mri burden of white matter lesions in people with multiple sclerosis: A systematic review and meta-analysis," *PloS one*, vol. 12, no. 5, p. e0177727, 2017.

[285] P. Sorrentino *et al.*, "Whole-brain propagation delays in multiple sclerosis, a combined tractography-magnetoencephalography study," *Journal of Neuroscience*, vol. 42, no. 47, pp. 8807–8816, 2022.

[286] M. F. Pinto *et al.*, "Prediction of disease progression and outcomes in multiple sclerosis with machine learning," *Scientific reports*, vol. 10, no. 1, p. 21038, 2020.

[287] F. Barkhof, "The clinico-radiological paradox in multiple sclerosis revisited," *Current opinion in neurology*, vol. 15, no. 3, pp. 239–245, 2002.

[288] J. Cabral *et al.*, "Metastable oscillatory modes emerge from synchronization in the brain spacetime connectome," *Communications Physics*, vol. 5, no. 1, p. 184, 2022.

[289] J. Makhalova *et al.*, "Virtual epileptic patient brain modeling: Relationships with seizure onset and surgical outcome," *Epilepsia*, 6 2022.

[290] H. E. Wang *et al.*, "Virtual brain twins for stimulation in epilepsy," *medRxiv*, 2024.

[291] H. E. Wang *et al.*, "Vep atlas: An anatomic and functional human brain atlas dedicated to epilepsy patients," *Journal of Neuroscience Methods*, vol. 348, p. 108983, 1 2021.

[292] B. Dollomaja *et al.*, "Virtual epilepsy patient cohort: generation and evaluation," *medRxiv*, 2024.

[293] S. Asadzadeh *et al.*, "A systematic review of eeg source localization techniques and their applications on diagnosis of brain abnormalities," *Journal of Neuroscience Methods*, vol. 339, p. 108740, 2020.

[294] G. Pellegrino *et al.*, "Source localization of the seizure onset zone from ictal eeg/meg data," *Human Brain Mapping*, vol. 37, pp. 2528–2546, 7 2016.

[295] S. Olmi *et al.*, "Controlling seizure propagation in large-scale brain networks," *PLOS Computational Biology*, vol. 15, p. e1006805, 2 2019.

[296] S. An *et al.*, "Optimization of surgical intervention outside the epileptogenic zone in the virtual epileptic patient (vep)," *PLOS Computational Biology*, vol. 15, p. e1007051, 6 2019.

[297] A. Horn *et al.*, "Connectivity predicts deep brain stimulation outcome in p arkinson disease," *Annals of neurology*, vol. 82, no. 1, pp. 67–78, 2017.

[298] T. Merk *et al.*, "Electrocorticography is superior to subthalamic local field potentials for movement decoding in parkinson's disease," *Elife*, vol. 11, p. e75126, 2022.

[299] M. Jakobs *et al.*, "Cellular, molecular, and clinical mechanisms of action of deep brain stimulation—a systematic review on established indications and outlook on future developments," *EMBO molecular medicine*, vol. 11, no. 4, p. e9575, 2019.

[300] W. C. Koller and M. G. Rueda, "Mechanism of action of dopaminergic agents in parkinson's disease," *Neurology*, vol. 50, no. 6_suppl_6, pp. S11–S14, 1998.

[301] A. Oswal *et al.*, "Neural signatures of hyperdirect pathway activity in parkinson's disease," *Nature communications*, vol. 12, no. 1, p. 5185, 2021.

[302] J. E. Rubin *et al.*, "Basal ganglia activity patterns in parkinsonism and computational modeling of their downstream effects," *European Journal of Neuroscience*, vol. 36, no. 2, pp. 2213–2228, 2012.

[303] A. Pavlides *et al.*, "Computational models describing possible mechanisms for generation of excessive beta oscillations in parkinson's disease," *PLoS computational biology*, vol. 11, no. 12, p. e1004609, 2015.

[304] O. Maith *et al.*, "A computational model-based analysis of basal ganglia pathway changes in parkinson's disease inferred from resting-state fmri," *European Journal of Neuroscience*, vol. 53, no. 7, pp. 2278–2295, 2021.

[305] J. M. Meier *et al.*, "Virtual deep brain stimulation: Multiscale co-simulation of a spiking basal ganglia model and a whole-brain mean-field model with the virtual brain," *Experimental Neurology*, vol. 354, p. 114111, 2022.

[306] R. P. Rocha *et al.*, "Recovery of neural dynamics criticality in personalized whole-brain models of stroke," *Nature Communications*, vol. 13, no. 1, p. 3683, 2022.

[307] T. U. Hauser *et al.*, "The promise of a model-based psychiatry: building computational models of mental ill health," *The Lancet Digital Health*, vol. 4, no. 11, pp. e816–e828, 2022.

[308] I. M. Berwian *et al.*, "Computational mechanisms of effort and reward decisions in patients with depression and their association with relapse after antidepressant discontinuation," *JAMA psychiatry*, vol. 77, no. 5, pp. 513–522, 2020.

[309] C. C. McIntyre and T. J. Foutz, "Computational modeling of deep brain stimulation," *Handbook of clinical neurology*, vol. 116, pp. 55–61, 2013.

[310] R. F. Betzel *et al.*, "Optimally controlling the human connectome: the role of network topology," *Scientific reports*, vol. 6, no. 1, p. 30770, 2016.

[311] A. I. Luppi *et al.*, "Contributions of network structure, chemoarchitecture and diagnostic categories to transitions between cognitive topographies," *Nature Biomedical Engineering*, pp. 1–20, 2024.

[312] I. R. Violante *et al.*, "Non-invasive temporal interference electrical stimulation of the human hippocampus," *Nature neuroscience*, vol. 26, no. 11, pp. 1994–2004, 2023.

[313] M. J. Wessel *et al.*, "Noninvasive theta-burst stimulation of the human striatum enhances striatal activity and motor skill learning," *Nature neuroscience*, vol. 26, no. 11, pp. 2005–2016, 2023.

[314] E. Acerbo *et al.*, "Focal non-invasive deep-brain stimulation with temporal interference for the suppression of epileptic biomarkers," *Frontiers in neuroscience*, vol. 16, p. 945221, 2022.

[315] E. Acerbo *et al.*, "Improved temporal and spatial focality of non-invasive deep-brain stimulation using multipolar single-pulse temporal interference with applications in epilepsy," *bioRxiv*, pp. 2024–01, 2024.

[316] K. K. Iyer *et al.*, "Focal neural perturbations reshape low-dimensional trajectories of brain activity supporting cognitive performance," *Nature communications*, vol. 13, no. 1, p. 4, 2022.

[317] R. Maran *et al.*, "Analyzing the brain's dynamic response to targeted stimulation using generative modeling," *arXiv preprint arXiv:2407.19737*, 2024.

[318] A. Ziaeemehr *et al.*, "Virtual brain inference (vbi): A flexible and integrative toolkit for efficient probabilistic inference on virtual brain models," *bioRxiv*, 2025.

[319] G. Papamakarios *et al.*, "Normalizing flows for probabilistic modeling and inference," *The Journal of Machine Learning Research*, vol. 22, no. 1, pp. 2617–2680, 2021.

[320] D. P. Kingma *et al.*, "An introduction to variational autoencoders," *Foundations and Trends® in Machine Learning*, vol. 12, no. 4, pp. 307–392, 2019.

[321] K. Barmpas *et al.*, "A causal perspective on brainwave modeling for brain–computer interfaces," *Journal of Neural Engineering*, vol. 21, no. 3, p. 036001, 2024.

[322] A. Payeur *et al.*, "Neural manifolds and learning regimes in neural-interface tasks," *bioRxiv*, pp. 2023–03, 2023.

[323] H. Hampel *et al.*, "The foundation and architecture of precision medicine in neurology and psychiatry," *Trends in Neurosciences*, vol. 46, p. 176–198, Mar. 2023.

[324] V. N. Vakharia *et al.*, "Computer-assisted planning for stereoelectroencephalography (seeg)," *Neurotherapeutics*, vol. 16, p. 1183–1197, Oct. 2019.

[325] M. Yu *et al.*, "The human connectome in alzheimer disease — relationship to biomarkers and genetics," *Nature Reviews Neurology*, vol. 17, p. 545–563, July 2021.

[326] Z. Yang *et al.*, "A deep learning framework identifies dimensional representations of alzheimer's disease from brain structure," *Nature Communications*, vol. 12, Dec. 2021.

[327] M. Frasca *et al.*, "Predicting parkinson's disease evolution using deep learning," 2023.

[328] J. M. Bower and D. Beeman, *The book of GENESIS: exploring realistic neural models with the GEneral NEural SImulation System*. Springer Science & Business Media, 2012.

[329] M. L. Hines and N. T. Carnevale, "Neuron: a tool for neuroscientists," *The neuroscientist*, vol. 7, no. 2, pp. 123–135, 2001.

[330] M.-O. Gewaltig and M. Diesmann, "Nest (neural simulation tool)," *Scholarpedia*, vol. 2, no. 4, p. 1430, 2007.

[331] D. F. Goodman and R. Brette, "The brian simulator," *Frontiers in neuroscience*, vol. 3, p. 643, 2009.

[332] K. Dai *et al.*, "Brain modeling toolkit: An open source software suite for multiscale modeling of brain circuits," *PLOS Computational Biology*, vol. 16, no. 11, p. e1008386, 2020.

[333] S. Heitmann *et al.*, "The brain dynamics toolbox for matlab," *Neurocomputing*, vol. 315, pp. 82–88, 2018.

[334] G. Ioannides *et al.*, "Spatiotemporal dynamics in spiking recurrent neural networks using modified-full-force on eeg signals," *Scientific Reports*, vol. 12, no. 1, p. 2896, 2022.